UNIVERSITY OF THESSALY

MASTER THESIS
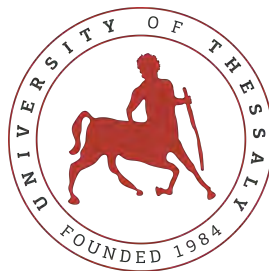
Study and Development of Wireless Networks for Distributed Sensing Infrastructures

Author:
PANAGIOTIS TZIMOTOUDIS

Supervisor:
Prof. ATHANASIOS KORAKIS

A thesis submitted in fulfillment of the requirements
for the degree of Master of Science in

Science and Technology of Electrical and Computer Engineering
Department of Electrical and Computer Engineering

October 30, 2020

Declaration of Authorship

I, PANAGIOTIS TZIMOTOUDIS, declare that this thesis titled, "Study and Development of Wireless Networks for Distributed Sensing Infrastructures" and the work presented in it are my own. I confirm that:

- This work was done wholly or mainly while in candidature for a research degree at this University.

- Where any part of this thesis has previously been submitted for a degree or any other qualification at this University or any other institution, this has been clearly stated.

- Where I have consulted the published work of others, this is always clearly attributed.

- Where I have quoted from the work of others, the source is always given. With the exception of such quotations, this thesis is entirely my own work.

- I have acknowledged all main sources of help.

- Where the thesis is based on work done by myself jointly with others, I have made clear exactly what was done by others and what I have contributed myself.

Signed:

_____

Date:

_____

Dedicated to my family and my friends…

Acknowledgements

First and foremost I wish to thank my advisor, Assistant Professor Thanasis Korakis for giving me the opportunity to work in such an inspiring research unit and more importantly for his guidance.

Also I would like to thank Assistant Professor Christos Antonopoulos and Assistant Professor Fotios Plessas, who are in my advisor commitee, for their guidance in this thesis.

Especially, I would like to thank my lab-mates in NITlab, for supporting me every day. First of all, I would like to thank Stratos Keranidis and Giannis Kazdaridis for supporting me from my first days in the lab and for our joint research and collaboration that we have all these years.

I would really like to thank Polychronis Symeonidis and Nikos Sidiropoulos for our collaboration in this work and moreover the rest NITLab members.

viii

Parts of this work presented in:

- Evaluation of lora performance in a city-wide testbed: Experimentation insights and findings [1], with co-authors: Giannis Kazdaridis, Stratos Keranidis, Polychronis Symeonidis, Ioannis Zographopoulos, Panagiotis Skrimponis, Thanasis Korakis

- The NITOS Wireless Sensor Network Testbed for Experimenting with Long-Range Technologies [2], with co-authors: Giannis Kazdaridis, Nikos Sidiropoulos, Polychronis Symeonidis, Thanasis Korakis

- and LoRa Mesh Network Experimentation in a City-Wide Testbed [3], with co-authors: Stratos Keranidis, Giannis Kazdaridis, Polychronis Symeonidis, Thanasis Korakis

UNIVERSITY OF THESSALY

Abstract

Faculty Name
Department of Electrical and Computer Engineering

Master of Science

**Study and Development of Wireless Networks for Distributed Sensing
Infrastructures**

by PANAGIOTIS TZIMOTOUDIS

In this thesis, we present a city-scale testbed and an in-lab testbed that employs several edge devices scattered across the urban area of our city, and in the floors of our University's premises to characterize the performance of long distance wireless protocols. The installation is augmented through a custom link quality evaluation framework that continuously monitors the Packet Delivery Ratio versus RSSI relation to characterize the performance of LoRa standard under realistic conditions. We are also evaluate the impact of implementing a CSMA/CA mechanism in LoRa protocol in order to boost the Packet Delivery Ration of the deployed links. Experimental results, collected over a period of several months, efficiently analyze LoRa's performance across a wide range of protocol configurations. Finally, we also present in-lab experiments that characterize the efficiency of LoRa modules in terms of power and energy efficiency per bit, along with valuable insights aimed at the development of energy efficient protocol improvements.

ΠΑΝΕΠΙΣΤΗΜΙΟ ΘΕΣΣΑΛΙΑΣ

Περίληψη

Τμήμα Ηλεκτρολόγων Μηχανικών και Μηχανικών Υπολογιστών

Μεταπτυχιακές Σπουδές

Μελέτη και Ανάπτυξη Ασύρματων Δικτύων σε Κατανεμημένες Υποδομές Αισθητήρων

του Παναγιώτη Τζιμοτούδη

Σε αυτή τη διατριβή, παρουσιάζουμε ένα testbed σε επίπεδο πόλης καθώς και ένα testbed το οποίο είναι τοποθετιμένο στους ορόφους του εργαστήριου μας με σκοπό τον χαρακτηρισμό της απόδοσης ασύρματων πρωτοκόλλων μεγάλων αποστάσεων. Η εγκατάσταση περιέχει επίσης ένα framework αξιολόγησης της ποιότητας των προσαρμοσμένων συνδέσμων (links) παρακολουθώντας συνεχώς την αναλογία παράδοσης πακέτων έναντι του RSSI για να χαρακτηριστεί η απόδοση του προτύπου LoRa υπό ρεαλιστικές συνθήκες. Επίσης, αξιολογούμε τον αντίκτυπο της εφαρμογής του μηχανισμού CSMA/CA στο LoRa πρωτόκολλο, προκειμένου να αυξήσουμε την αναλογία παράδοσης πακέτων των αναπτυσσόμενων συνδέσμων. Τα πειραματικά αποτελέσματα, που συλλέχθηκαν σε διάστημα αρκετών μηνών, αναλύουν αποτελεσματικά την απόδοση του LoRa σε ένα ευρύ φάσμα διαμορφώσεων του πρωτοκόλλου. Τέλος, παρουσιάζουμε πειράματα που πραγματοποιήθηκαν στο εργαστήριο και χαρακτηρίζουν την αποδοτικότητα των LoRa μονάδων σε σχέση με την ισχύ και την ενεργειακή απόδοσης ανά μονάδα μεταδιδόμενης πληροφορίας, μαζί με πολύτιμες γνώσεις που στοχεύουν στην ανάπτυξη ενεργειακά αποδοτικών βελτιώσεων του πρωτοκόλλου.

Contents

xiv

List of Figures

xvi

List of Tables

List of Abbreviations

AS	**Application Server**
BW	**Bandwidth**
BPS	**Bits Per Second**
CCA	**Clear Channel Assesement**
CR	**Coding Rate**
CRC	**Cyclic Redundancy Check**
CSMA	**Carrier-Sense Multiple Access**
CSMA/CA	**Carrier-Sense Multiple Access with Collision Avoidance**
CSS	**Chirp Spread Spectrume**
DCF	**Distributed Coordinated Function**
EIRP	**Effective Isotronic Radiated Power**
ETSI	**Europena Telecommunications Standards Institute**
FSK	**Frequency Shift Keying**
IoT	**Iinternet of Things**
ISM	**Industrial Scientific Medical**
JS	**Join Server**
LBT	**Listen Before Talk**
LPWA	**Low-Power Wide-Area**
LPWAN	**Low-Power Wide-Area Netowrk**
MAC	**Medium Access Control**
NS	**Network Server**
OTA	**Over-The-Air**
PDR	**Packet Delivery Ratio**
PHY	**Physical Layer**
SF	**Spreading Factor**
ToA	**Time on Air**

Chapter 1

Introduction

In the latest years, a lot of research has been done in the area of wireless networks for distributed sensing infrastructures. The trend of Internet of Things (IoT) has spread fluently and has gained a lot of interest in both academic studies as also in industrial developments. Nonetheless, more research needs to be conducted in order to exploit and to obtain the full potential of the available technologies and protocols.

In this work, we will be focusing on technologies which provide long-range communications for monitoring scenarios focusing in smart cities and smart metering. Since 2013, these technologies are widely known as Low-Power Wide-Area (LPWA) technologies [4]. These novel group of technologies offer long-range communication with notably low power consumption. They have emerged because traditional wireless networks are not suitable for these use cases, neither low consumption nor long-range.

Specifically, the common characteristics of Low-Power Wide-Area Network, mentioned in [5] and listed below:

– Low power consumption because devices are generally powered by batteries.

– Chips are inexpensive and rapid to deploy.

– Easy and scalable deployment.

– ALOHA with single hop routing is the preferred technique to control medium access.

– Radio modulation must be robust to channel fading.

– Data must be secured.

There are a lot of existing LPWAN technologies, where some of them operate in the unlicensed spectrum bands while some more are operate in licensed bands from the 3GPP [6]. In the unlicensed area, LoRaWAN is the most highlighted since there are many successful deployments in real-world and it emerges as the leading solution because of its easy deployment and open nature, a detailed discussion of LoRaWAN will be in chapter 2. Another popular technology in this area is Sigfox [7], which is managed by a single operator and offers a complete IoT architecture very constrained by the amount of data using a proprietary UNB modulation. Finally, in the unlicensed area, two more options exist, DASH7 [8] and Weightless [9]. These two options are less popular, but both of them have a higher impact on the research domain as both of them are open standardized stacks.

In the case of licensed bands from the 3GPP, there are two well-known LPWAN technologies, NB-IoT [10] and LTE-M [11]. The NB-IoT exploits the existing cellular network to connect devices which generate small data flow. In special cases, where applications require more data to send and more often, LTE-M will be more suitable

as it provides a wider bandwidth. A comparison between LPWAN technologies and other well-known communication technologies in terms of power comparison and range coverage is illustrated in Figure 1.1.
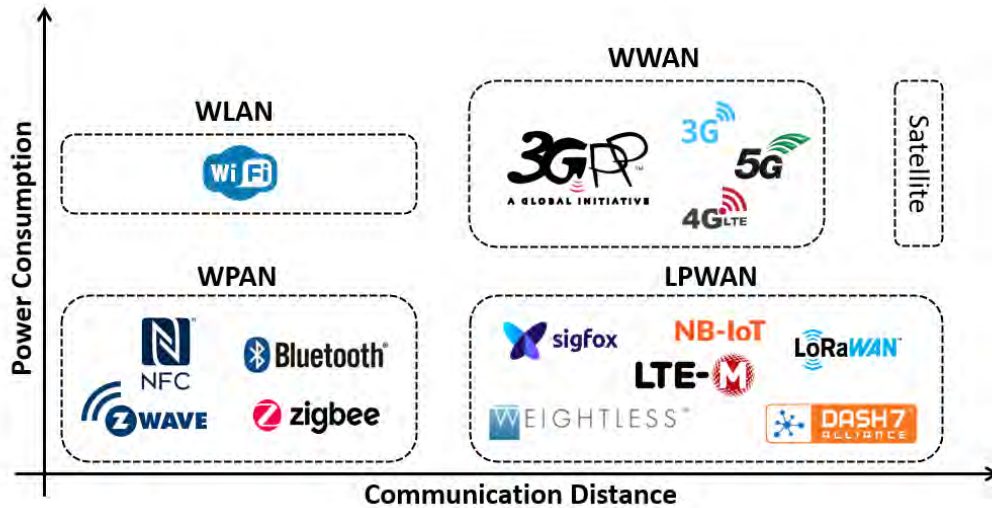
FIGURE 1.1: Comparison of wireless technologies in terms of power consumption and range coverage.

Most of these LPWAN technologies are currently used in many situations, but all have the same common drawback, only single-hop communication is supported. This means that for large areas, it is necessary to deploy infrastructure for unlicensed technologies or to pay a telephone provider for using base stations. This problem is exacerbated in urban areas, where physical phenomena such as interference and obstacles reduce the coverage range to a few kilometres. In addition, LoRa has no mechanism for collision avoidance which will probably lead to increased packet loss. As pointed in [12], where the number of devices increases to 250 and the packet size is 50 bytes, the probability of successful transmission decreases to 10% due to collisions.

The main contribution of this work is to characterize the energy efficiency of LoRa SX1272 chipsets and the performance of the LoRa protocol in terms of uplink PDR. Furthmore, we adapt and implement the CSMA/CA mechanism from 802.15.4, and we characterize the performance of LoRa protocol when the CSMA/CA is applied under the isolated wireless NITOS testbed. To this aim, we divide this document into three chapters. The remaining of this work is organized as follows:

- **LoRa**

  The theoretical background of LoRa modulation is described here as long as the description of LoRaWAN network. A distinction between them is made, and the specifications of both are explained.

- **Testbed** Our testbed setup is defined here, alongside its hardware components. The topology and the architecture of our testbed is also described here.

- **Experimentation**

  The experiments that we conducted are presented here alongside the findings that we discover. Firstly, we characterize the LoRa protocol in terms of energy consumption and energy consumption per bit. After that we characterize

the link performance in our city-wide testbed. Also, we conduct extensive experiments in our in-lab testbed in order to define the impact o concurrent transmissions in PDR when two edge nodes operate at the same or at different channels. Lastly, we evaluate the performance of LoRa protocol in terms of uplink PDR when a CSMA/CA mechanism is applied.

- **Conclusion and future work**

  Finally, in this chapter, we conclude our work quoting the key points of this thesis, while we point a few interesting paths for future work.

Chapter 2

LoRa

In 2020, ten years after the first introduction of LoRa technology, an amount of over 100 million devices has been implemented. This long-range and low power technology was invented by Nicolas Sornin and Olivier Seller in 2010 when they started a start-up company named Cycleo together with François Sforza [13]. Their primary goal was to provide a modulation technique for gas and water monitoring as long as electricity metering in wide areas. Two years later, an American company called Semtech collaborated with Cycleo, and they launched together the first chipsets with LoRa modulation. Two chicpsets SX1272/73 [14] and SX1276 [15] was implemented for end devices and the SX1301 [16] for the gateways.

Following this, the LoRa Alliance [17] was founded in 2015, and they introduced the LoRaWAN protocol. LoRaWAN established a new standard for Low-Power Wide-Area Networks (LPWANs) in order to define message formats and security aspects as long as to enable the networking in the upper layers. LoRA Alliance is an open and non-profit fast-growing technology alliance. Their goal is to provide an association between companies, research groups such as universities and developer communities in order to collaborate and share knowledge with the goal of foster and standardize the LPWAN using LoRaWAN, guaranteeing interoperability among different operators.

2.1 LoRa PHY

The LoRa technology, a proprietary physical layer (PHY) modulation technique, is based on Chirp Spread Spectrum (CSS). A digital communication spread spectrum technique uses wideband linear frequency modulated chirp pulses to encode information. That kind of modulation is capable of transmitting signals over long distances, and it is fairly robust against interference. LoRa modulation has four main configuration parameters: the operation channel, the channel bandwidth (BW), the spreading factor (SF) and the coding rate (CR).

2.1.1 Channel

LoRa utilizes channels in the license-free sub-GHz ISM (Industrial, Scientific, Medical) bands. The usage of these license-free bands and their respective regulations differ by region. As indicated in [18], there are six common channel plans based on the operational region and are listed in Table 2.1 alongside with their respective regulations.

In this thesis, we are focusing on the EU868 ISM band as we are in Europe. In Europe, the ISM radio spectrum used in LoRa is defined by the European Telecommunications Standards Institute (ETSI) [19]. By the ETSI standard, the band ranges between 863 and 870 MHz and imposes some restrictions regarding the transmission

Region	Channel Plan	Channel Range	Duty Cycle	Max TX Power
Europe	EU868	863-870 MHz	1% *	14 dBm
US	US915	902-928 MHz	1%	14 dBm
China	CN470	470-510 MHz	1%	14 dBm
Australia	AU915	915-928 MHz	1%	14 dBm

TABLE 2.1: ISM Bands.

power and the maximum time the transmitter can be on. The transmission power ($T_X Power$) is limited to $+14dBm$ while the maximum duty cycle is limited to 1% but according to the ETSI regulations it is allowed to use a Listen Before Talk (LBT) transmission management mechanism in order to overcome the restriction of 1% in duty cycle.

2.1.2 Bandwidth

The LoRa utilizes wide bandwidths (BW) ranging in values 125, 250 and 500 kHz [14]. The value of the BW indicates how wide the transmission signal will be, as long as the duration of the transmission and the sensitivity. The 500 kHz value is better for faster transmissions but lacks in communication range and sensitivity. On the other hand, the 125 kHz value ends up to higher time-on-air but it can perform better communication range and the sensitivity of the signal is better, so the communication has a better link budget.

2.1.3 Spreading Factor

The representation of each bit of payload information by multiple chips of information is performed in the spread spectrum LoRa modulation [14]. This variation of frequency can take discrete values inside the frequency channel which are defined by the spreading factor (SF). The spreading factor is the number of chips per symbol used in the data treatment before the transmission signal. The SF can take values in range of 7 - 12 but there exist special cases where the value can be 5 or 6. Then we can define the symbol rate R_s and the bit rate R_b as follows:

$$R_s = \frac{BW}{s^{SF}}, R_b = SF * \frac{BW}{2^{SF}}$$

Considering the BW and SF parameters affecting the resulting physical (PHY) layer data rate, er configure the full list of available settings (BW and SF), presented in Table 2.2.

Spreading Factor (SF)	Bandwidth (BW)		
	125 kHz	250 kHz	500 kHz
7	6835	13671	27343
8	3906	7812	15625
9	2197	4394	8789
10	1220	2441	4882
11	671	1342	2685
12	366	732	1464

TABLE 2.2: Data Rate (bps) regarding the SF and BW configurations.

2.1.4 Coding Rate

The last parameter that can be configured in LoRa modulation is the coding rate. LoRa modem performs cyclic forward error detection and correction to further improve the robustness of the link [14]. The coding rate can be set to either 4/5, 4/6, 4/7 or 4/8. Such error coding adjoins a transmission overhead. In Table 2.3 below, the additional data overhead per transmission is shown. Note that the data rate presented in Table 2.2 will be affected by the coding rate and the actual data rate that we will get in transmission will be subtracted by the overhead ratio of the configured coding rate.

Coding Rate (CR)	Overhead Ratio
4/5	1.25
4/6	1.5
4/7	1.75
4/8	2

TABLE 2.3: Coding Rate (CR) overhead.

2.1.5 Packet Format

Except for the modulation technique, LoRa also establishes the format of the physical packet. LoRa supports two types of operation packet format, explicit and implicit [14]. In explicit header mode, the packet includes a short header after the preamble part of the packet, that contains useful information about the number of bytes, packet's coding rate but also a flag that indicates whether a CRC is used in the packet or not. In detail, as illustrated in Figure 2.1 packet type comprises of three parts:

- **Preamble**

  The preamble is an initial group of symbols and it is used in order to synchronize the receiver to the incoming data flow. The value of the symbols sequence is a programmable variable and and it can get values from 6 to 65535, yielding to a total preamble length of $6 + 4$ to $65535 + 4$ symbols. The default value is configured to 12 symbols long sequence and it is mandatory to configured identically in both in receiver and transmitter in order to get a correct reception.

- **Header**

  This part of the packet is optional and provides information on the payload such as the payload length in bytes, the coding rate used for encoding the payload, and the presence or not of the optional 16-bit CRC for the payload. Apart from the payload that encoded in a user-defined coding rate, the header is always encoded using the coding rate of 4/8. This part of the packet is present only in explicit mode.

- **Payload**

  The payload is the part of the packet that contains the actual data that encoded based on the chosen coding rate. The payload is a variable-length field but it is limited to a maximum of 255 bytes. The optional value of CRC may be appended at the end of the payload.
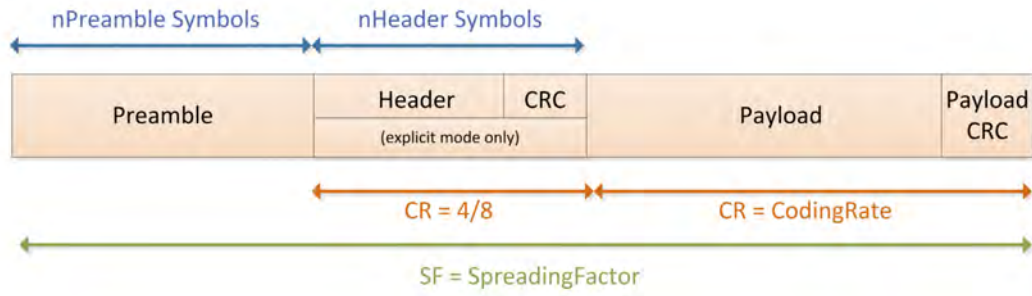
FIGURE 2.1: LoRa packet format. Retrieved from [14].

2.1.6   Time on Air

Using a specific combination of bandwidth (BW), spreading factor (SF), and coding rate (CR) it is simple to calculate the total time on air of a LoRa packet. It will be useful to define the symbol rate T_s for a given nominal symbol rate R_s as:

$$T_s = \frac{1}{R_s}$$

In order to calculate the time on air of a LoRa packet, we need to calculate two separate parts of the packet. Firstly, we need to calculate the duration of the preamble part of the packet, which is calculated as follows:

$$T_{preamble} = (n_{preamble} + 4.25) * T_s$$

Where $n_{preamble}$, is the programmed preamble length. Secondly, we need to calculate the duration of the rest of the packet which includes both the payload part and the optional header part. This duration is proportional to the number of the symbols $n_{payload}$ and it is calculated as follows:

$$n_{payload} = 8 + max\left(\left\lceil \frac{8 * PL - 4 * SF + 28 + 16 * CRC - 20 * IH}{4 * (SF - 2 * DE)} \right\rceil * (CR + 4), 0\right),$$

$$T_{payload} = n_{payload} * T_s$$

Where PL is the number of payload bytes, CRC is a boolean variable that indicates the presence of CRC at the end of the packet or not, IH is a boolean variable that is used to indicate the usage of the implicit or explicit header, DE is a boolean variable that indicates if the low data rate optimization is enabled or not and lastly, the CR is the coding rate variable that can get values from 1 to 4 based on the coding rate that has been chosen. Finally, the total time on air (ToA) of a LoRa packet, is simply the sum of the duration of the two parts:

$$T_{packet} = T_{preamble} + T_{payload}$$

2.2   LoRaWAN

The link layer of LoRa LPWANs primarily developed under a proprietary license by Semtech and referred to as LoRaMAC. Following this, an open-source MAC layer

protocol called LoRaWAN created by LoRa Alliance [17]. This MAC protocol operates on top of the LoRa physical (PHY) layer and it is defined in LoRaWAN specification [20].

The architecture of LoRaWAN networks is based on a star-of-stars topology as illustrated in Figure 2.2. The end nodes which operate in a single channel communicate directly to every multi-channel gateway in reach. Gateways act as a transparent bridge between end nodes and the back-end forwarding all packets received to a network server using an Internet connection such as Ethernet, WiFi, or Cellular (3G, 4G).
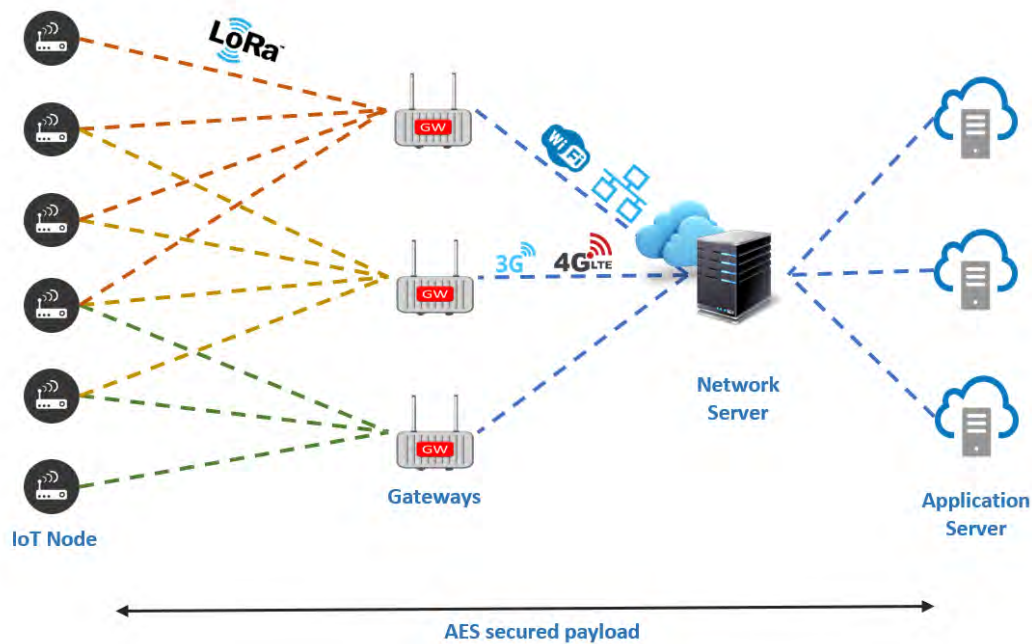

FIGURE 2.2: LoRaWAN® architecture.

2.2.1 Gateways

Gateways are intermediate devices that have implemented a packet forward layer in order to convert LoRa physical (PHY) packets to standard IP packets. Also, should perform the opposite action which allows bidirectional communication. Alongside, gateway devices should be able to communicate simultaneously in all combinations of channels and spreading factors, improving network capacity, and provide the flexibility for frequency hopping. Finally, this type of devices should be always powered on to provide a reliable service to the network.

2.2.2 End-nodes

In order to provide flexibility in terms of energy consumption, to support a wide range of LoRa applications, LoRaWAN defines three different types of end-devices. The key difference between these types of devices is the receive window timing that they have in order to listen to downlink messages from the gateway. The three device types that defined by LoRaWAN according to [20] are listed below:

- **Class A**

These kinds of devices are the most energy-efficient devices. While it sends an uplink message it stays in receive mode for exactly two short timeslots for downlink messages. In this way, it provides the opportunity for bidirectional communication or receives commands, but simultaneously can keep the energy cost at the minimum value. Class A must be implemented by all LoRaWAN end-nodes because it is the base for the rest classes.

- **Class B**

  In this class, we have the same behavior as the class A devices with the addition of one extra scheduled timeslot for the reception. This timeslot is scheduled using a beacon packet from the gateway, given the ability to synchronize the downlink packet with the receive windows of the end node.

- **Class C**

  These devices are the most energy-consuming devices. Unlike from the other two devices are always on receive mode except when they transmitting a packet. Based on that, they have the minimum latency for downlink messages among the three classes, but they have a low operation lifetime because of the high power consumption.

2.2.3   Back-end Architecture

As detailed in [21] LoRaWAN back-end is composed of several micro-services. It is well defined that the overall back-end comprised of three units listed below:

- **Network Server**

  The network server (NS) is the end of the LoRaWAN MAC layer and it will be characterized as the center of the star topology of the network. It's key responsibilities or features are the end-device address checking, the frame authentication, and the acknowledgments that send to the end-devices. Also, it is responsible for the data rate adaptation, for all MAC layer requests generating from end-devices and also for the queuing of the downlink messages generating from the Application Server to the end-devices that is connecting to the network. Finally, the NS is responsible for the forwarding of all Join-request and Join-accept messages that have been exchanged between the join server and the end nodes.

- **Join Server**

  The join server (JS) unit of the back-end is responsible for the authentication of end-devices and it manages the Over-the-Air (OTA) activation process. In this unit is stored all the necessary items that been used in order to identify securely an end node. The JS must establish a secure connection with the network server, while it is possible to be connected in multiple NSs at the same time.

- **Application Server**

  The application server (AS) unit is the part of the back-end that is connected to the end-user. It is responsible for handling all the application features such as the managing of the packets for both the uplink and downlink messages, providing an application layer service to the end-users. The application server must share with the JS the application credentials. An AS could be connected

to multiple NSs at the same time and vice versa, and it could be connected to multiple JSs.

2.2.4 Regional Parameters

Finally, as mention and in 2.1.1 LoRa utilizes channels in the license-free sub-GHz ISM bands and must respect the regulations within the region of its operation. To this end, LoRaWAN specification also considers the spectrum usage in different regulatory regions worldwide, and a list of the available channel plans based on the region of its operation are summarized in Table 2.4.

Region	Channel Plan	Common Name
Europe	EU863-870	EU868
United States	US902-928	US915
China	CN779-787	CN779
Europe	EU433	EU433
Australia	AU915-928	AU915
China	CN470-510	CN470
Japan	AS923	AS923
South Korea	KR920-923	KR920
India	IN865-867	IN865
Rusia	RU864-870	RU864

TABLE 2.4: Worldwide frequency channel plans.

As in this thesis, we will operate in the region of Europe, we will focus on the EU863-870 channel plan as it is the most common plan in European countries. In contrast to the EU433, which has no frequency plan yet, the EU868 is regulated under the ETSI standard. In this context, LoRaWAN specifies a minimum of three supported channels for all devices (868.1 MHz, 868.3 MHz, and 868.5 MHz) with the restriction of duty cycle at 1%. Besides, a maximum EIRP, which is the radiated output power of end nodes, is limited to 16 dBm. A full list of the available combinations of modulation type, spreading factor, and bandwidth presented in Table 2.5 alongside with the physical data rates that they can achieve.

Modualation	Spreading Factor (SF)	Bandwidth (kHz)	Data Rate (bps)
LoRa	12	125	250
LoRa	11	125	440
LoRa	10	125	980
LoRa	9	125	1760
LoRa	8	125	3125
LoRa	7	125	5470
LoRa	7	250	11000
FSK	12	125	50000

TABLE 2.5: TX data rate table for EU863-870 channel plan.

Chapter 3

Testbed

Experimentation under real-world settings is deemed essential when evaluating new protocols and algorithms in order to derive to safe results. During the last decade, several institutions developed large-scale set-ups focused on wireless sensor networks experimentation. SmartSantander [22] is a pioneering facility, counting a few thousands nodes deployed in the city of Santander in order to facilitate smart-city applications. On the other hand, w-iLab.t [23] provides a large-scale testbed deployed in an indoor environment allowing for reproducible experiments using short-range technologies. In the same page, FIT IoT-lab [24] accommodates several distinguished sites across France, again for testing short-range technologies in indoor spaces. Another remarkable work is the FlockLab [25] testbed, suggesting that every sensor node is equipped with an *"observer"* board, responsible for obtaining power consumption measurements and marking timestamps in various events when they occur.

Apparently, the main wireless IoT technologies employed by the aforementioned testbeds are short-range communication protocols, such as IEEE 802.15.4 and BLE, while lately, many of the them are upgrading their infrastructure to support the recently introduced Low-Power WAN (LPWAN) technologies, such as NB-IoT, LoRa and LoRaWAN that exhibit huge potential. These standards use a physical layer that sacrifices throughput performance, supporting throughput speeds ranging from hundreds of bits to a few kilobits per second, to provide long range communication in the order of tens of kilometers. In fact, entire cities can be covered with the utilization of only one Gateway node on top of it.

In this work, we develop a remotely controllable and configurable setup based on long-range protocols that can be used on both city-wide and in-lab testbeds.

3.1 Device Setup

Each device consists of three major components: an embedded device, a custom-designed PCB board with monitoring features, and an IoT node attached with a LoRa interface.

3.1.1 Embedded Device

The Embedded Device used is the BeagleBone Black Rev. C board [26] which is a low-cost, embedded platform characterized by sufficient processing power capabilities (ARM Cortex-A8 Processor at 1 GHz with 512 MB RAM) and several I/O pins, while it also embeds an Ethernet port for communicating with the backbone network. Of course, a WiFi version is also available for connecting to wireless networks instead of wired and it is used in out city-wide testbed in locations where the wired connection was not available. Figure 3.1(a) illustrates a BeagleBone Black

with an Ethernet port for communication, while Figure 3.1(b) illustrated the wireless version of the embedded device.
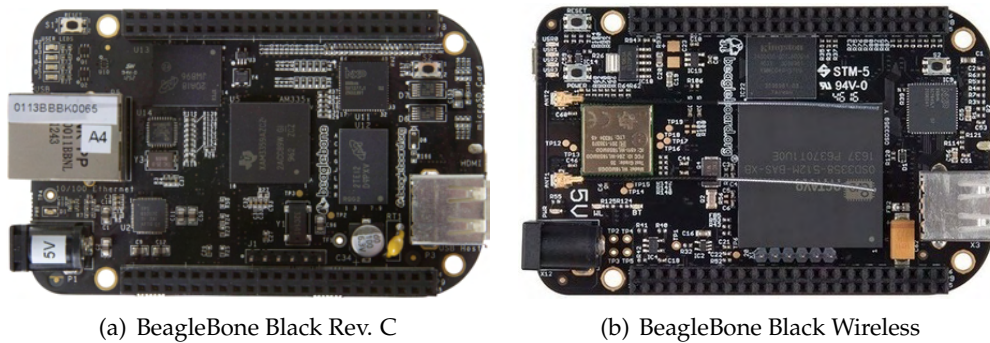

(a) BeagleBone Black Rev. C   (b) BeagleBone Black Wireless

FIGURE 3.1: BeagleBone Embedded Device

3.1.2   IoT Node

As IoT node we use two options illustrated in 3.2. Firstly, we use the Waspmote sensor device produced by Libelium [27], which is designed to work with extremely low power consumption. This device features a low power ATmega1281 microcontroller operating at 14.74 MHz. It embeds high-speed Flash memory of 128 KB, an EEPROM of 4KB and an SRAM of 8 KB. Moreover, it integrates an XBee-footprint socket for plugging-in wireless interfaces, such as LoRa, ZigBee, BLE, etc. while extra sensing modules can be interfaced through the available I2C and I/O ports. Figure 3.2(a), illustates a waspmote sensor device attached with a LoRa SX1272 transeiver.

Secondly, a custom designed ICARUS mote [28], illustrated in Figure 3.2(b), is used. The ICARUS mote features the ultra-low power STM32L476RG which is an ARM Cortex-M4 32-bit RISC core MCU operating at a frequency of up to 80 MHz. It embeds high-speed Flash memory of 1 MB and an SRAM of 128 KB. Moreover, it embeds a SHT21 temperature humidity, a VEML6030 light intensity and a MAX17048G+ battery gauge sensors, while extra sensing modules can be interfaced through the available I2C and I/O ports. The mote integrates an XBee-footprint socket for plugging-in wireless interfaces, such as LoRa, ZigBee, BLE, etc., In our setup ICARUS features a LoRa transceiver that integrates the SX1272 [14] chipset manufactured by Semtech paired with a 4.5 dBi antenna.
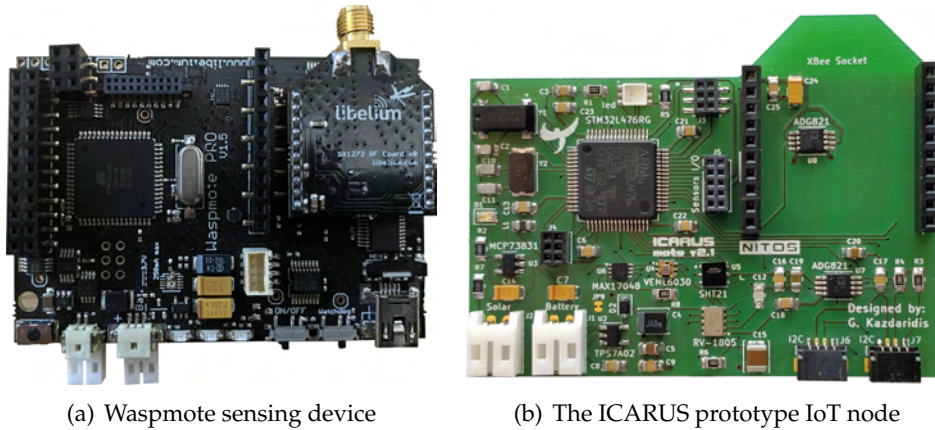
(a) Waspmote sensing device (b) The ICARUS prototype IoT node

FIGURE 3.2: IoT nodes

3.1.3 LoRa Interface

As it was mentioned before, the LoRa technology was invented by Semtech and implemented into the LoRa transceivers family. In particular, the most common one is the single-channel and single-SF SX1272 chip [14]. Figure 3.3(a) illustrates an XBee-footprint implementation by Libelium that integrates the SX1272 chipset. Another common design, is the RF-LoRa alternative from the RF Solutions [29] as illustrated in Figure 3.3(b), which is integrated to an XBee-footprint PCB board by us.
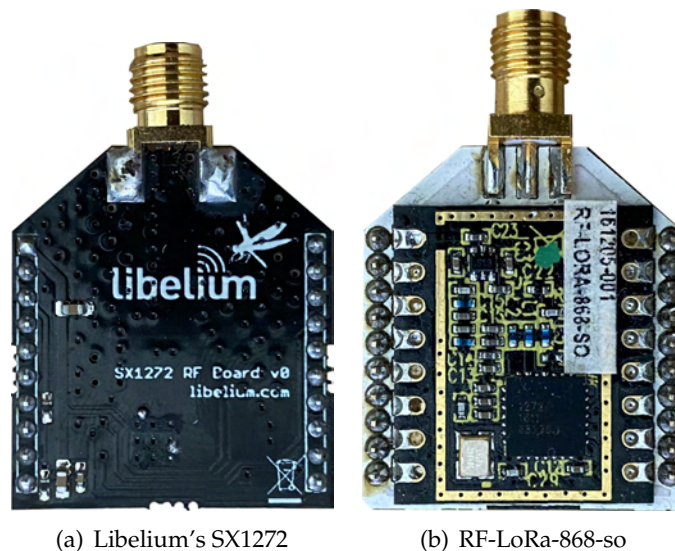

(a) Libelium's SX1272 (b) RF-LoRa-868-so

FIGURE 3.3: LoRa interfaces

In order to work with them, the first possibility is to connect any microcontroller to the modules using the SPI interface. This is a very low-cost choice to get to know the technology and reuse compatible old devices, such is the case of an Arduino board or our custom made ICARUS mote.

3.1.4   End Node

Connecting all the components together, we build our custom made end nodes as illustrated in Figure 3.4. In our setup we use an ST-Link programmer to remotely upload firmware to the sensing nodes as well as to monitor their program execution through a serial port. Furthermore, we use the BeagleBone board to measure the power draw of the IoT node in real-time in order to characterize new protocols in terms of energy-efficiency. To this aim, we employ our custom-designed PCB board (cape) that integrates the required electronic components presented in [30, 31, 32]. Specifically, the monitoring board features several power monitoring channels that are capable of operating in parallel, thus we fix it to monitor both the entire node's consumption as well as individually the power draw of the LoRa interface. Additional components can also be monitored with the required hardware interventions.

FIGURE 3.4: Testbed node

3.2   Remote Contol

Creating a WSN testbed, it is important to provide flexibility in terms of reconfigure basic properties and means to easily extract data from the network. To this end, we develop a system that gives to the users the ability to remote control the end IoT nodes through the embedded device attached to our end nodes. Moreover, the logs that specified by the end user, such as the operational status or variety of execution status of the IoT nodes, forward from the end node to our InfluxDB instance on our server. This feature, gives the ability to the researchers to retrieve data from the experimentation execution in an easy way.

The architecture of our remote control system is presenting in Figure 3.5. Starting from the right, the IoT node is connected to the embedded device, of the end

node, via a serial port. The usage of this connection is two fold. Firstly, it is used for uploading a compatible executable file to the IoT node. Secondly, it offers the ability for monitoring the program execution. The end node, apart of controlling the IoT node, is always connected with our server and is responsible for relay all the execution messages produced from the node to our server in order to be persist on our InfluxDB instance. The end node sends the logging messages using MQTT messages. Additionally, the end node is always be suscribed to specific MQTT topics waiting commands from the server regarding the execution of the IoT node as long as to upload a new compatible file to the node.

As illustrated in the middle, the server the server is the heart of our testbed. Except of the responsibility of persist the log messages produced by the IoT nodes in the database, it handles all the requests from the users. If an upload request come from the user, the server is responsible for uploading it to the desired end node and then an automatically procedure is started in order to flash the executable file to the IoT node. Finally, the server is always connected to with end nodes in order to obtain information regarding the operation status of the nodes.

FIGURE 3.5: Remote control architecture

The control panel of our WSN testbed, which is the interface with the uses is presenting in Figure 3.6. Using this panel the user can get usefull information about the network topology as as show on the top left of the figure. Additionally, the user can acquire inforamtion regarding the node id, the type of the IoT node that is deployed, and the network interface of each node. Moreover, can get information about the operation status which can been changed through the start and the stop button. Finally, in case the operation status of the IoT node is idle or ready, the user can upload to the selected node a custom compatible executable file.

For uploading the custom compatible file to the IoT node we follow the following procedure.

- Once the user select its file it automatically saved to our server after a quick check if the file type is correct.

- The end end node notified from the server for an upload request through a MQTT message.

- The end node connects to the server and download the new file using a secure file transfer protocol
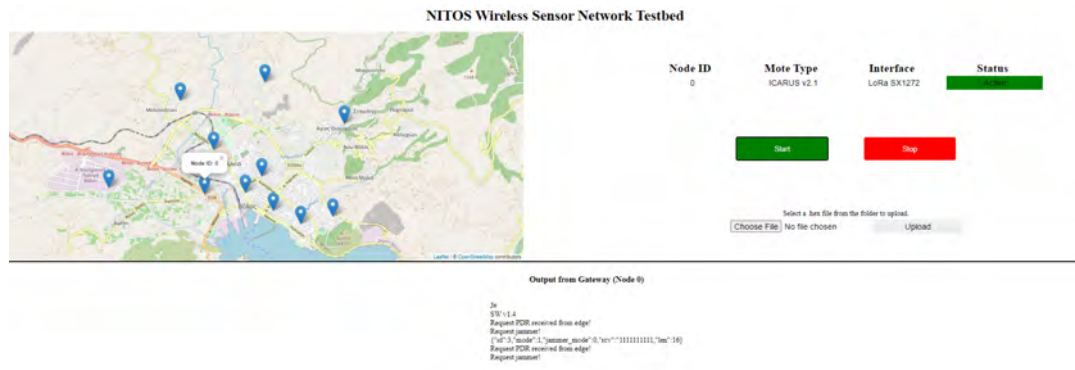
FIGURE 3.6: Wiresless Sensor Network Testbed front-end

- After the download procedure ends the uploading procedure to IoT node is starting.

- Finally, when the uploading procedure is finished the end node notifies the server regarding the new state of the IoT node using an MQTT message.

3.3   City-wide Testbed

Our city-wide testbed consists of a total of eleven end nodes. In order to characterize our network, we declare one of them as the gateway node, as it is deployed on the rooftop of our University's premises and the remaining nodes which are scattered across the city of Volos as end nodes. Figure 3.7 illustrates the testbed topology, while the characteristics of each individual end device are presented in Table 3.1.
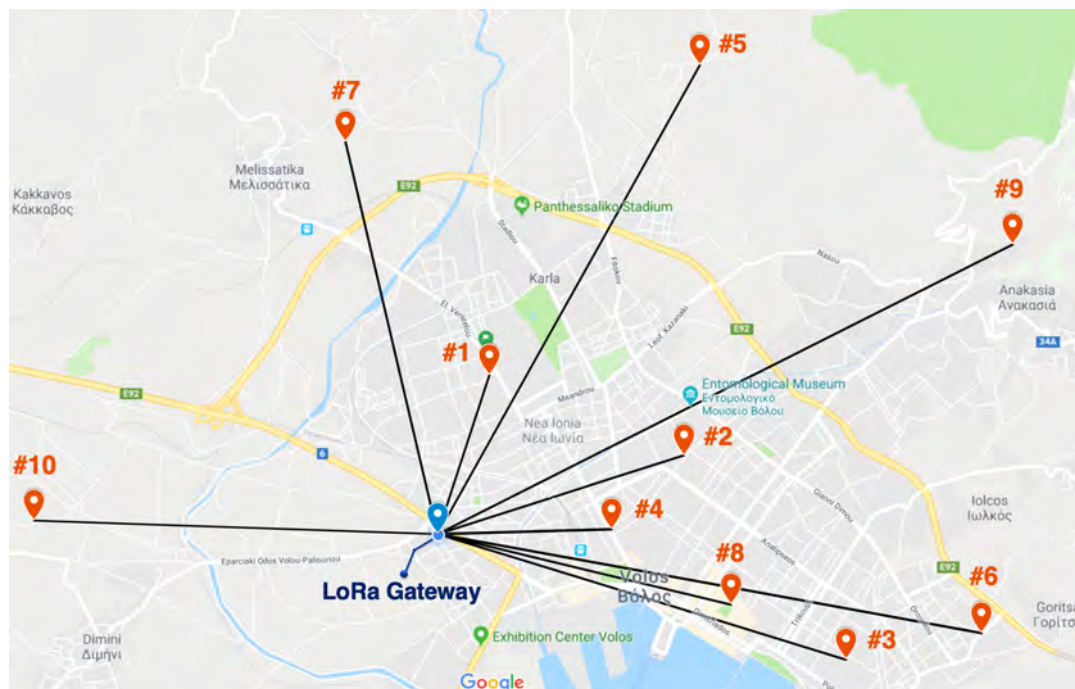
FIGURE 3.7: City-wide testbed topology

We clearly observe that the testbed offers a wide range of wireless links that differentiate in terms of communication distance, elevation difference and LOS/NLOS conditions.

ID	GW Distance (km)	Altitude (m)	LOS/NLOS
GW	-	23	-
1	1.3	43	NLOS
2	1.98	30	NLOS
3	3.25	32	NLOS
4	1.33	25	NLOS
5	4.12	179	LOS
6	4.22	55	NLOS
7	3.11	128	LOS
8	2.32	35	NLOS
9	4.92	170	LOS
10	3.10	8	NLOS

TABLE 3.1: City-wide testbed node characteristics

3.4 In-Lab Testbed

Alongside of our city-wide testbed we deemed necessary to build and an in-lab testbed in order to characterize the inter-build communications of LoRa. To this end, we deployed eight more end nodes scatter to our University's building as illustrated in Figure 3.8. We deploy two end nodes to each floor of our building between second and fourth floor, and two end nodes on the under-ground garage station, while we use the same end node, as in our city-wide testbed, as the gateway node which is deployed in the rooftop of the building.
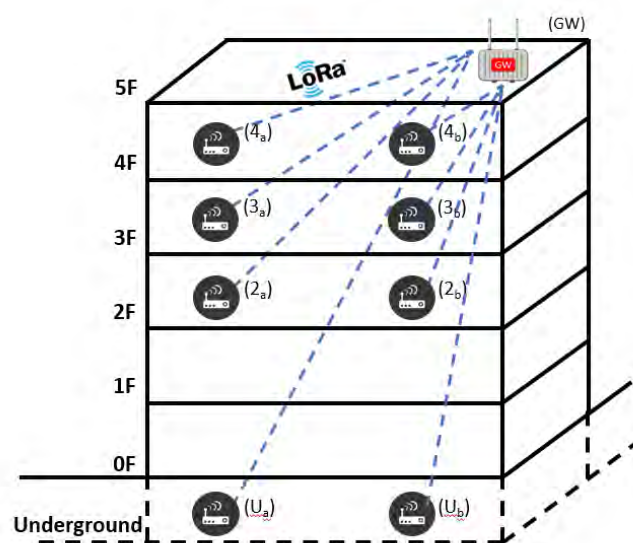
FIGURE 3.8: In-lab testbed topology

3.5   Link Quality Evaluation Framework

Implementing a WSN testbed to evaluate the performance of a wireless technology, it is important to build a tool that can evaluate the performance of the employed communication links. To this end, we design a link quality evaluation framework that continuously capture traces of the packet delivery ration (PDR) versus RSSI of the employed communication links.

The overall procedure is orchestrated at the gateway (GW) level, which periodically polls the different end nodes that continuously remain in receive mode. The list of the end nodes is a configurable parameter by the experimenter in order to evaluate the exactly nodes that his willing of. Nodes polling is executed in a Round-robin fashion, instructing end node to participate in a link quality evaluation experiment. Upon receiving a request for experiment, each end node transmits ten consecutive packets at the data rate, payload length and transmission power that has been determined by the GW. Data rate, payload length and transmission power are configurable values and take values in range of 1-10 (based on tx mode as presenting in Table 3.2), 5-250 bytes and 0 - 14 dBm respectively. The gateway sends the experiment settings embedded to the experiment request packet. The per-node link quality of the network is determined through the Packet Delivery Ration of the aforementioned experiments and continuously persisted in the InlfuxDB that is accessible over remote API for further evaluation.

Considering the parameters that affecting the resulting PHY layer data rate, we configure the full list of available setting of bandwidth, spreading factor and coding rate, by using the list of combinations presented in Table 3.2. For simplicity, we refer to these combinations as Transmission Modes from 1 to 10. Additionally, Table 3.2 lists the resulting sensitivity and indicative airtime for each Transmission Mode, using a reference payload size of 10 Bytes.

Transmission Mode	BW (kHz)	SF	Data Rate (bps)	Sensitivity (dBm)	Airtime (msec)
1	125	12	293	-137	1155.07
2	250	12	586	-135	577.53
3	125	10	977	-133	329.72
4	500	12	1172	-129	288.76
5	250	10	1954	-130	164.86
6	500	11	2149	-128	164.86
7	250	9	3516	-128	82.43
8	500	9	7032	-122	41.21
9	500	8	12500	-119	23.16
10	500	7	21875	-116	11.58

TABLE 3.2: LoRa Transmission Mode characteristics

Chapter 4

CSMA for LoRa

The absent ability to perform carrier-sense on off-the-shelf LoRa end devices has impeded studies and implementations of the suitable Carrier-Sense Multiple Access (CSMA) schemes for LoRa. Currently, the LoRa networks, including those organized in an ad-hoc manner or by following the LoRaWAN specification, adopt an ALOHA media access control (MAC) mechanism to access communication mediums defined by radio frequency and the spreading factor (SF) of the chirp spread spectrum (CCS) modulation. Although ALOHA allows a simple network implementation, it is not competent with keeping up with the increasing demand of IoT devices added to the ISM band. For this reason, even though devices may conform to channel usage limitations (e.g., 0.1% or 1% duty cycle in Europe), the ALOHA-based LoRa networks will have degraded network performance due to massive collisions when the numbers of end devices grow sharply in this era of IoT.

Several studies have analyzed the potential benefit of Carrier-Sense Multiple Access (CSMA) for LoRa-based networks [33, 34, 35]. In [33], the authors proposed carrier sense multiple access CSMA protocol with LoRaWAN and simulated on NS-3 where they sense channel 10 ms before sending every packet. Using this approach, they improved the collision ratio whereby utilising a sample of large number of devices. Their protocol also consumes less energy as compared to LoRaWAN, while using more than 5000 devices in a network. In [34], the authors have assessed a range of channel access control protocols and demonstrated by means of simulation that CSMA is scalable and the best amongst those considered in terms of reliability and energy consumption for a high node count. The authors in [35] investigate through simulations the LoRa scalability utilizing CSMA as a substitute of ALOHA-based medium access of LoRa.

However, there is very little information on the practical performance of LoRa CSMA over longer distances. Only, C. Pham in [36] perform a practical evaluation of CSMA for long LoRa payloads between 2 nodes. First, a protocol was adapted from the IEEE 802.11 Distributed Coordinated Function's (DCF) basic CSMA mechanism. It was found that this mechanism becomes unreliable with increased range which impacts negatively in a real-world deployment. An extended DCF Inter-Frame Space (DIFS) was suggested and defined as the maximum transmission ToA in which periodic carrier detection was performed.

4.1 IEEE 802.11

Among many CSMA variants, the one implemented in the IEEE 802.11 (WiFi) is quite representative of the approach taken by most of random access protocols with so-called backoff procedure. Figure 4.1 illustrates the IEEE 802.11 CSMA mechanism used in the basic Distributed Coordinated Function (DCF) mode which is the

common operation mode of WiFi networks with a base station. The basic DCF IEEE 802.11 CSMA/CA (Collision Avoidance) works as follows:

- A node senses the channel to determine whether another node is transmitting before initiating a transmission

- If the medium is free for a DCF inter-frame space (DIFS) the transmission will proceed

- If the medium is busy, the node defers its transmission until the end of the current transmission and waits an additional DIFS before generating a random number of backoff slot time in the range [0, W - 1].

- The backoff timer is decreased as long as the medium is sensed to be idle, and frozen when a transmission is detected on the medium, and resumed when the channel is detected as idle again for more than DIFS

- When the backoff reaches 0, the node transmits its packet

- The initial W is set to 1. W is doubled for each retry (exponential backoff) until it reaches a maximum value
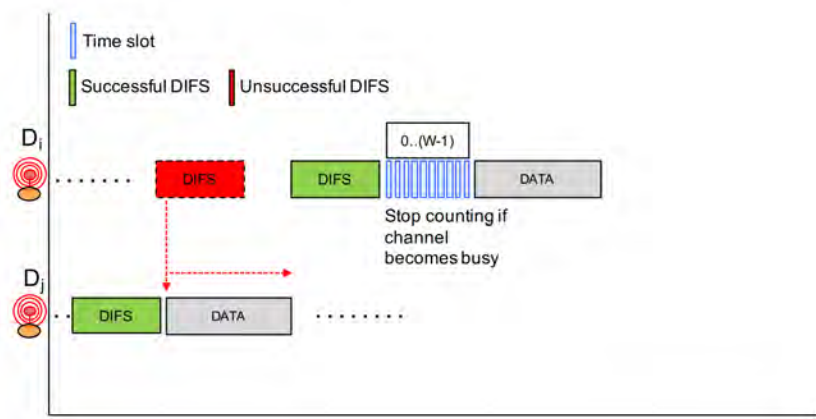
FIGURE 4.1: CSMA/CA algorithm as defined in 802.11. Retrieved from [36]

The random backoff timer is applied after a busy channel because it is exactly in that case that the probability of a collision is at its highest value. This is because several users could have been waiting for the medium to be available again

4.2   IEEE 802.15.4

Closer to the domain of IoT, IEEE 802.15.4, that was very popular for wireless sensor networks (WSN), proposes both non-beacon-enabled mode with unslotted CSMA/CA channel access mechanism and beacon-enabled networks with slotted CSMA/CA. Here, we are describing the non-beacon-enabled mode (as shown in Figure 4.2) as the beacon-enabled needs a coordinator and higher level of synchronization that is definitely not suited for LoRa IoT networks.

- Before a transmission, a node waits for a random number of backoff periods in the range $[0..2^{BE} - 1]$. BE is set to 3 initially

- If at the end of the waiting time the medium is sensed to be free the transmission will proceed

- If the medium is busy, the node defers its transmission, increases BE until it reaches a maximum value and waits for an additional $[0..2^{BE} - 1]$ backoff periods
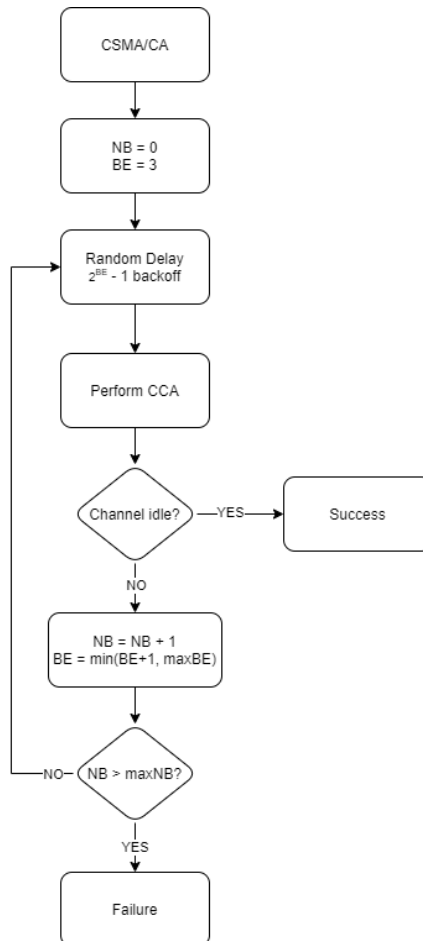
FIGURE 4.2: CSMA/CA algorithm as defined in 802.15.4

IEEE 802.15.4 always implements a backoff timer prior to any transmission and simply increases the backoff timer interval each time the channel is found busy for the same packet, without constantly checking the channel to know when it is going back to idle.

Chapter 5

Experiments

Extensive LoRa communication experiments were conducted within our city-wide and in-lab testbeds located in Volos, Greece. In the following experiments, we highlight the performance of LoRa protocol under a wide range of settings and features to provide detailed performance analysis and cross-comparisons.

5.1 LoRa Power Consumption

Firstly we characterize the power consumption profile of the LoRa SX1272 chipset, under various protocol configurations. The experiments are conducted in the lab, employing a set of a transmitter and a receiver. To measure power draw, we place a small shunt resistor (1 Ω) between the IoT node's regulated power supply (3.3 Volts) and the SX1272's input supply pin. The voltage drop across this resistor is proportional to the current draw of the LoRa interface, which we measure with our high-end power consumption monitoring tool, presented in [30, 37]. The measurements were obtained with 100 MHz sampling speed at resolution of16 Bits that provides the required level of detail. To characterize specific events, such as packet transmission or reception, we isolate the respective part of the measurements and calculate the average value.

5.1.1 Instantaneous current consumption

In the first experiment, we characterize the instantaneous current consumption profile of the SX1272 LoRa chipset, during frame transmission and reception under various TX_P and TX_M settings.

Specifically, we configure the LoRa chipset in all available configurations, firstly in transmission mode and then in reception mode and we isolate the respective events in order to measure their instantaneous current draw.

The results of the first experiment are illustrated in Fig. 5.1(a) where the TX_P increases from *0 dBm* to *+7 dBm* and *+14 dBm*, while using the fixed TX_M setting of the first rate configuration and a payload size of *10 Bytes*. Similarly, in Fig. 5.1(b) we set the TX_P to *+14 dBm* and vary the TX_M to all the available rate configurations from 1 to 10. In this plot we use a fixed payload size of 100 Bytes and we clearly observe that the relation between the duration of each frame propagated and the transmission speed of each TX_M is inversely proportional as expected. We repeat the same experiment but this time we configure the LoRa chipset as a receiver and we measure the instantaneous power draw, as illustrated in Fig. 5.1(c). We can observe the variation in instantaneous power consumption in each different TX_M. Notably, the red line illustrated in Fig. 5.1(a), Fig. 5.1(b) and Fig. 5.1(c) represents the average power draw calculated as a moving mean over a window of 100 values in an effort to provide a more representative indication to derive safe results, since the

(a) Varying TX_P, in TX_M 1

(b) Current cons. in T_X, across different TX_M, employing +14 dBm TX_P
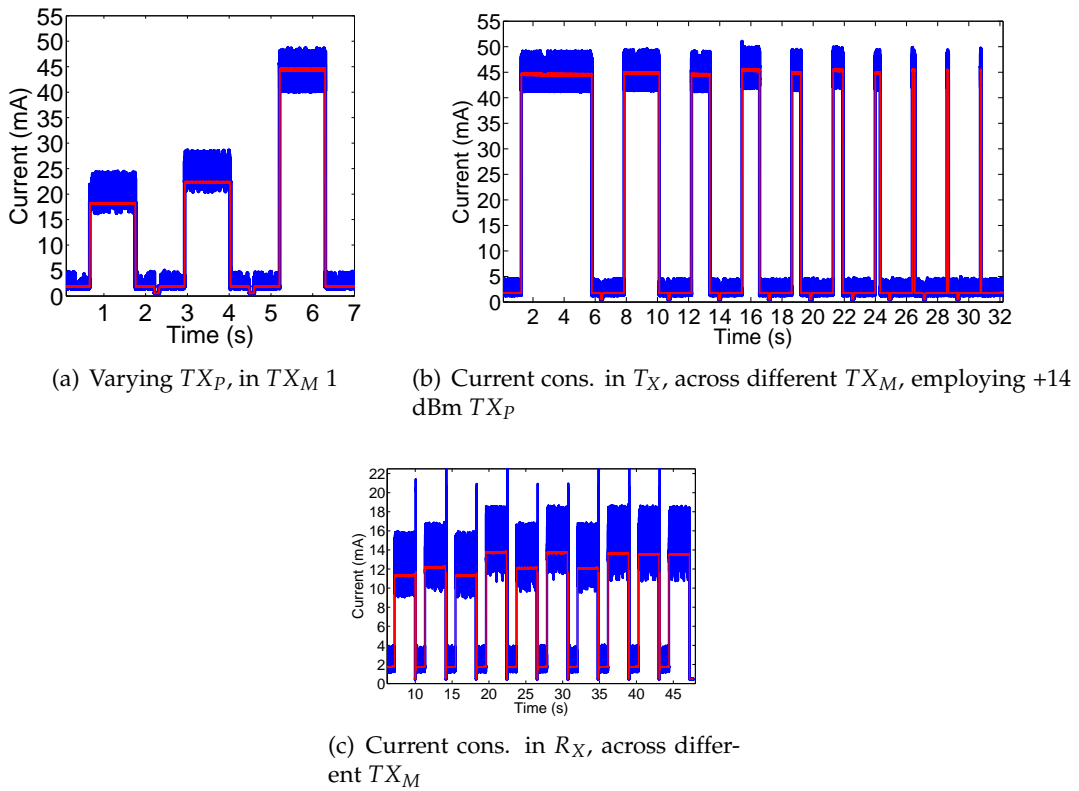
(c) Current cons. in R_X, across different TX_M

FIGURE 5.1: Obtained Current Consumption measurements

obtained measurements present high variations. Finally, the sudden drops from idle state to zero between each packet transmission or other spikes illustrated are related to the re-configuration of the LoRa parameters executed prior to each transmission or reception.

The analytic results across all tested parameters are listed in Table 3.2. We clearly observe that switching from the *+14 dBm TX_P* (*44.64 mA*) to the *+7 dBm TX_P* (*22.13 mA*), we can reduce current consumption by *50.43 %*, while marginal decrease of *14.33 %* is obtained when switching from *+7 dBm* to *0 dBm TX_P*. Both observations are made for the first TX_M configuration. Considering the whole set of TX_M configurations the reduction varies at the same levels, specifically in the case of switching from the *+14 dBm* to the *+7 dBm TX_P* it varies from *50.43 %* (*TX_M: 1*) to *49.42 %* (*TX_M: 4*), while in the case of *+7 dBm* to *0 dBm TX_P* we obtain a variation from *14.45 %* (*TX_M: 7*) to *13.78 %* (*TX_M: 6*). It is worth noting that the differentiation among the different TX_P levels, stems from the fact that a Power Amplifier (PA) circuit block is engaged in order to amplify the propagated signal, which in some cases drains the most of the total power [38]. The latter, suggests that it is preferable to use *+7 dBm TX_P* instead of *0 dBm*, to achieve sufficiently higher PDR at almost the same energy cost in scenarios where required higher link budget.

The obtained results also highlight the impact of TX_M parameter in power consumption under the same TX_P. Relating consumption data with *BW* and *SF* parameters of Table 3.2, it is made clear that the *BW* parameter plays significant role in the resulting draw, while *SF* configurations merely impact the obtained current consumption. We observe that TX_M configurations with fixed *BW* present roughly stable power draw. For instance when employing *BW* of 125 KHz (which is realized

in TX_M *1* and *3*) the power consumption remains exactly the same under the same TX_P setting. Whilst, in the rest *BW* configurations of 250 KHz and 500 KHz the power consumption variation under the same *BW* and TX_P settings does never exceed *1* %, which further highlights that the *BW* parameter totally affects the resulted power draw, while *SF* setting plays minor role. Notably, the highest obtained draw variation under the same TX_P is *4.47* % for the *0 dBm* TX_P, *4.01* % for the *+7 dBm* and *2.03* % for the *+14 dBm*. It is worth noting that the adjacent TX_M 5 and 6 present significant draw variation despite the fact they present marginal difference in their attained data rates, *1.954 kbps* and *2.149 kbps* respectively. Specifically, they present 3.08 % current increase.

Identical findings can be drawn when using reception mode (RX_P), where the impact of *BW* is even more highlighted. More specifically, during reception, we note a decrease of 11.54 % when switching from *500 KHz BW* (TX_M: *4*) to *250 KHz* (TX_M: *2*) and the remarkable variation of *18.9* % when switching from *500 KHz* (TX_M:*4*) to *125 KHz* (TX_M:*1*). Notably, the same variations in TX_M during transmission in the max TX_P provides marginal power consumption decrease of up to *2.03*%. This clearly shows that the power draw of the reception mode, is even more affected by the employed *BW* configuration, which is also noticeable by Fig. 5.1(b).

5.1.2 Energy Efficiency per Bit

As frame transmission duration is monotonically related to the configured data rate, it is important to quantify energy efficiency in terms of energy consumption per transmitted bit of information (E_B), as analyzed in our previous works [39, 40], which focus on analyzing the efficiency of the WiFi protocol. We calculate E_B, expressed in *Joules/bit*, as the division of the power consumption values collected for each different TX_M and TX_P by the exact *data rate* value.

In Fig. 5.2, we plot the obtained transmission E_B across the available *data rate* configurations and zoom in on the first 7 TX_M settings. We plot the E_B for the payload sizes of *14, 44 and 255 Bytes*, while we omit the case of *24 Bytes* for space reasons. Notably, the dashed lines on the plots represent the respective *data rates* of each TX_M. We notice that higher *data rate* settings always result in lower E_B, which is mainly due to the decreased duration of frame transmissions. The only two cases that present different behavior are the adjacent pairs *3, 4* and *5, 6*. We observe that the calculated E_B in TX_M *4* is marginally higher than that of TX_M *3*, which is also true for TX_M *6* and TX_M *5*. This happens since, TX_M *4* and *6* present higher draw than *3* and *5* respectively, while the achieved data rates are nearly equal. This finding suggests skipping TX_M *3* and *5*, and proceeding to TX_M *4* and *6* respectively, when considering energy efficient rate adaptation algorithms. Moreover, the highest observed variation is up to *15.12* % when comparing the pair of TX_M *5* and *6*, realized in the *+14 dBm* setting when transmitting packets of *14 Bytes* payload and *9.98* % and *11* % for the cases of *44* and *255 Bytes* respectively. Regarding the comparison of the calculated E_B among the illustrated payload sizes we observe an extreme variation. More specifically, when comparing the E_B of *14 Bytes* payload with the one of *44 Bytes* under the TX_M *1* the reduction is *90.14* %. Whilst, the difference is even bigger when comparing the *14 Bytes* with the *255 Bytes* under the TX_M *1*, with reduction reaching up to *98.99* %.

Similarly, we plot the E_B under varying payload sizes in the reception phase, in Fig. 5.3, by zooming in on the first 7 TX_M. The obtained measurements present identical behavior for TX_M *3, 4* and *5, 6* as in the transmission phase. To note that the variation of the E_B for the pairs TX_M *3, 4* and *5, 6* is even higher than the ones in

(a) Energy / bit in T_X, employing 14 Bytes Payload (b) Energy / bit in T_X, employing 44 Bytes Payload

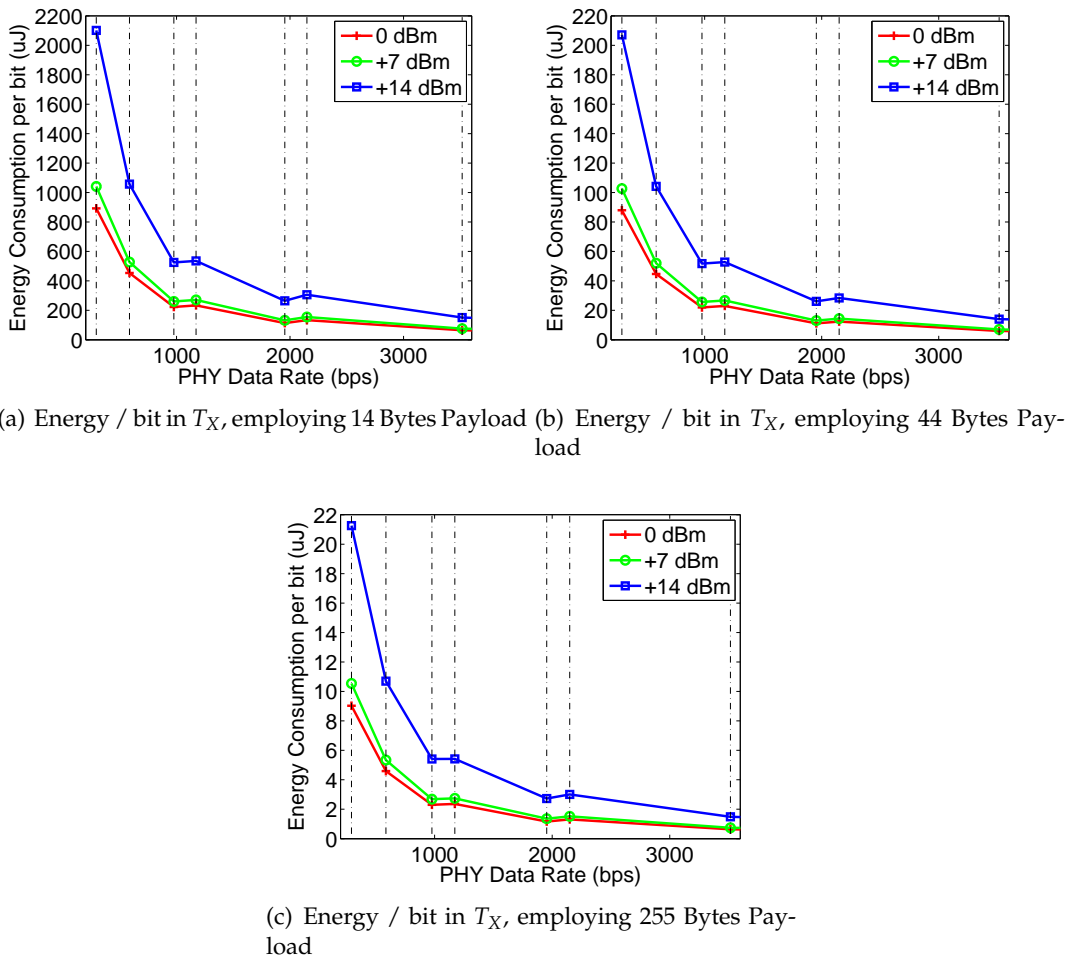(c) Energy / bit in T_X, employing 255 Bytes Payload

FIGURE 5.2: Energy Efficiency per bit measurements in T_X mode across different Payload sizes

the transmission phase. Namely, it is *27.33 %*, *19.17 %* and *11.35 %* for the cases of *14, 44* and *255 Bytes* respectively, when considering the pair TX_M *5* and *6*. Thus, we further highlight the urge to omit the TX_M *3* and *5*, and select the TX_M *4* and *6* when designing power efficient rate adaptation algorithms. Direct comparison of the E_B among payload sizes of *14, 24* and *44 Bytes*, during reception, presents remarkable energy efficiency improvement of *71 %* and *90 %* respectively. The variation is even higher when comparing payloads of *14* and *255 Bytes*, reaching up to *99.78 %*. This finding, highlights the fact that measurement aggregation techniques can achieve extremely improved energy efficiency in LoRa setups.

Assuming an energy experiment based on our deployed network, in which the sensor nodes propagate their measurements once per hour, we can estimate the lifetime of the network on typical batteries and compare it with the same experiment when employing aggregation mechanisms. In a scenario where a node is propagating *14 Bytes* of information using the maximum TX_P setting, we can calculate that the LoRa chipset will consume roughly *140 mAh* of the total power budget in a year, if we assume ideal conditions in sleep mode and wake-up operation. Considering a power budget of *400 mAh* dedicated only for LoRa transmissions the module's lifetime will be approximately *2.87* years. When employing an aggregation mechanism,
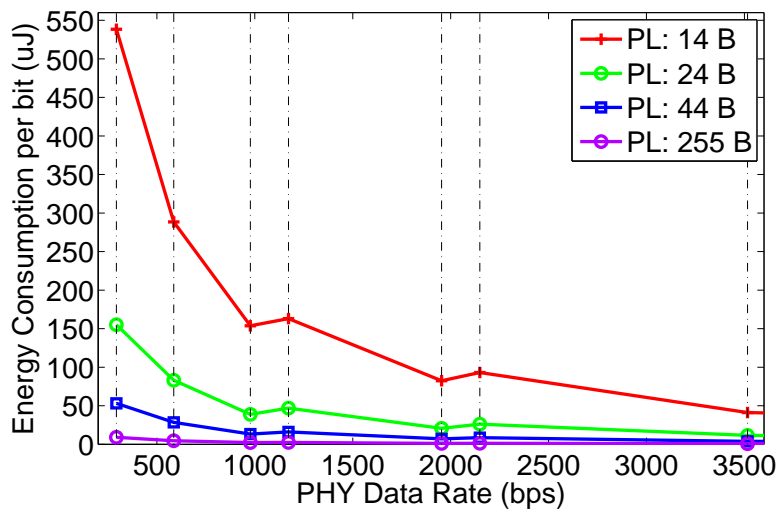
FIGURE 5.3: Energy Efficiency per bit measurements in R_X mode
across different Payload sizes

grouping several individual measurement frames into a single *100 Bytes* packet the consumed power will be *62 mAh* in a year, which suggests lifetime of roughly *6.38* years. The latter implies an increase of *122* % in lifetime, while aggregation using *255 Bytes* frame will lead to an increase of *160* % in lifetime.

5.2 Link Performance Evaluation
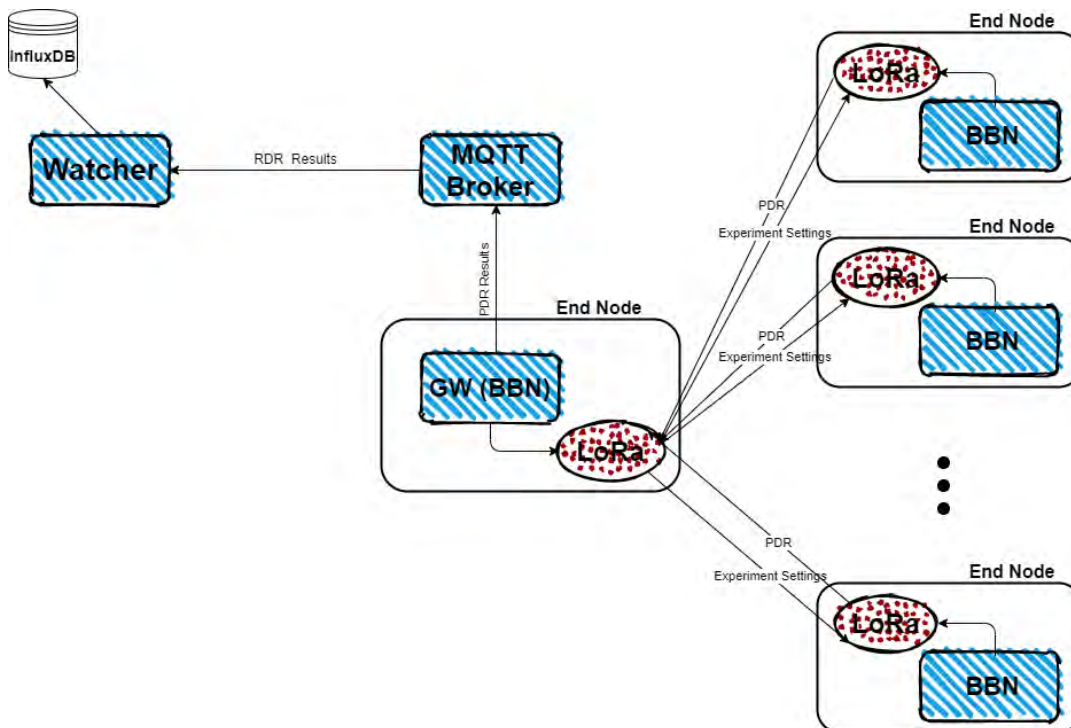
FIGURE 5.4: Link performance evaluation architecture

This section presents a thorough analysis of LoRa performance across a wide range of conducted testbed experiments, under uplink communication initiated from by each one of the *10* nodes and destined to the *GW*. The architecture of our testbed experimnets presented in Figure 5.4. The list of varying parameters (Table 3.2) corresponds to a total of *1200* experimental combinations that are conducted every hour, corresponding to *24K* frames transmitted per day. The resulting large dataset includes measurements collected over a period of *2* months. In order to effectively visualize the wide set of collected measurements, we decided to group the node and TX_P combinations, in terms of the resulting *RSSI* per link, thus LoRa performance is evaluated in terms of *PDR* and spans the *RSSI* range between *-102* and *-137 dBm*.

Figures 5.5(a), 5.5(b) and 5.5(c) illustrate the *PDR* performance versus uplink *RSSI* and TX_M, across the *3* different tested payloads. The solid lines correspond to the different TX_M (Table 3.2), while the dashed lines refer to the corresponding sensitivity thresholds, as calculated employing payload of *10 bytes* [41] compared to the ones calculated through our realistic experiments (*14 Bytes, 44 Bytes and 255 Bytes*). Considering the results across increasing payload sizes, we clearly see that the obtained sensitivity thresholds tend to increase (at maximum by *1 dB* per step), which also verifies the validity of the experimental results.

(a) Payload length 14 Bytes

(b) Payload length 44 Bytes

(c) Payload length 255 Bytes
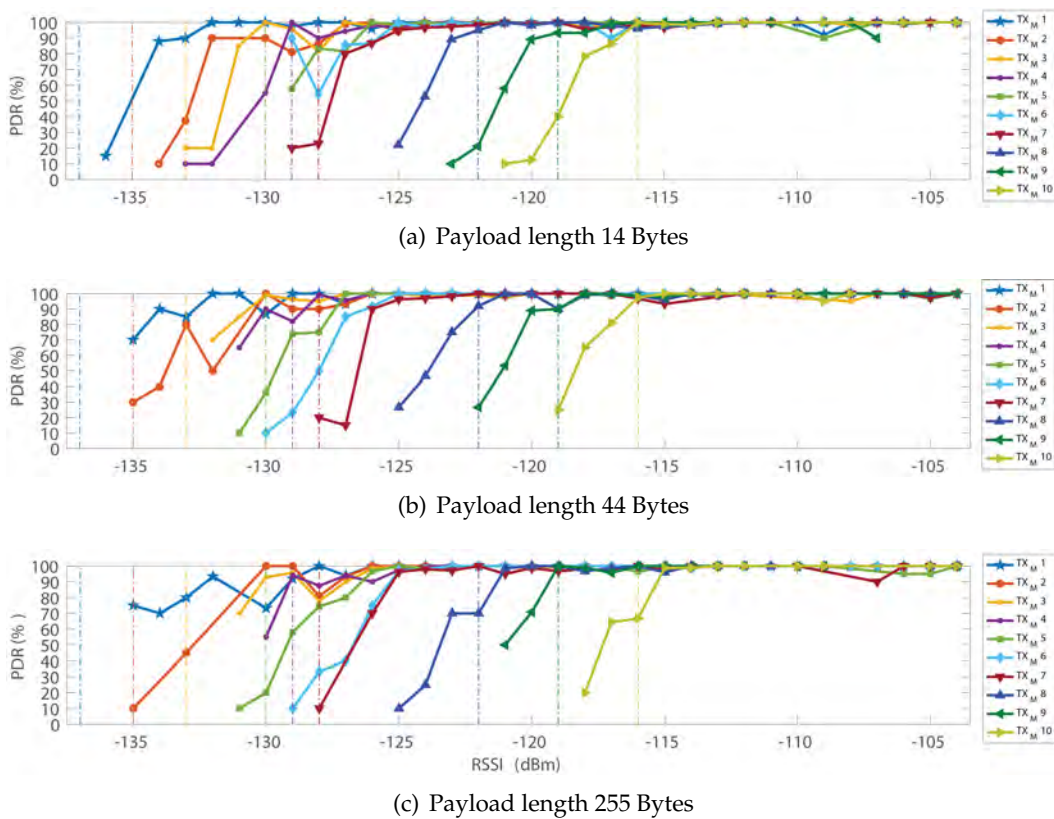
FIGURE 5.5: LoRa PDR performance versus uplink RSSI and TX_M

In the extreme cases employing the TX_M *1* and *10*, we observe the remarkable performance of LoRa achieve approximately *90% PDR* at *-134 dBm* and *-118 dBm* *RSSI* for transmissions at TX_M *1* and *10* respectively, under realistic city-scale experiments. Focusing on the maximum payload case, we can observe that even *-115 dBm* LoRa links are able to transfer frames of *255 Bytes* at TX_M *10* with approximately

100% PDR that is able to achieve *21.89 Kbps* and can support the transferring of low-quality images or even video streams in real-time. Relating this insight with Fig. 5.6, we notice that *8* out of the *10* considered links are able to support such demanding applications in the maximum TX_P setting.
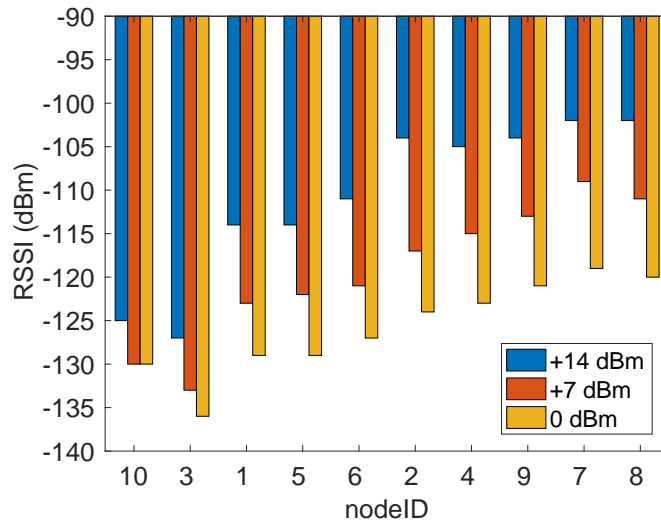
FIGURE 5.6: Uplink RSSI per LoRa link across different TX_P levels (*0, +7, +14 dBm*)

In the rest of this section, we attempt to define the optimal mapping of *RSSI* to TX_M, when considering the *30* different link scenarios (*10 nodes in 3 different TX_P levels*), as depicted in Fig. 5.6. Following a heuristic approach commonly employed in rate adaptation mechanisms, we identify the best *PHY* layer setting, as the maximum setting able to maintain higher than *90%* of *PDR*. Fig. 5.8 illustrates the mapping of TX_M to the *30* link types, considering the aforementioned rate selection principle. We clearly see that most of the tested links for the *0 dBm* TX_P level, are able to maintain higher than *90%* of *PDR* for TX_M higher than *4* for *RSSI* levels higher than *-129 dBm*. On the other hand, considering the maximum TX_P setting (*+14 dBm*), we notice that most links can maintain the TX_M of *7* for *RSSI* levels higher than *-114 dBm*. Only *6* out of *30* tested links, generated from nodes *3* and *10*, correspond to link quality lower than *-127 dBm* and require the configuration of lower TX_M settings. The sum of collected results highlight the potential of LoRa to achieve stable communication performance for data rates much higher than the basic one, across a wide range of low quality links.
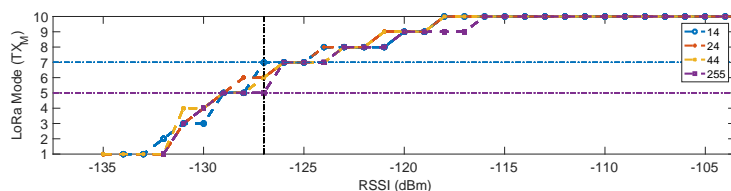
FIGURE 5.7: LoRa mode versus uplink RSSI and payload length

Finally, in Fig. 5.7, we illustrate the detailed mapping of $RSSI$ to TX_M, considering the varying frame payload parameter as well. It is made clear that the transmission of larger frames, requires the increase of TX_M, by up to two levels, as in the case of *-127 dBm*, which corresponds to results collected from nodes *3 and 6* under TX_P accordingly. Concluding, we remark that the wide range of collected results highlights the importance of employing automated rate adaptation for LoRa communication that jointly considers the varying $RSSI$ and payload parameters.
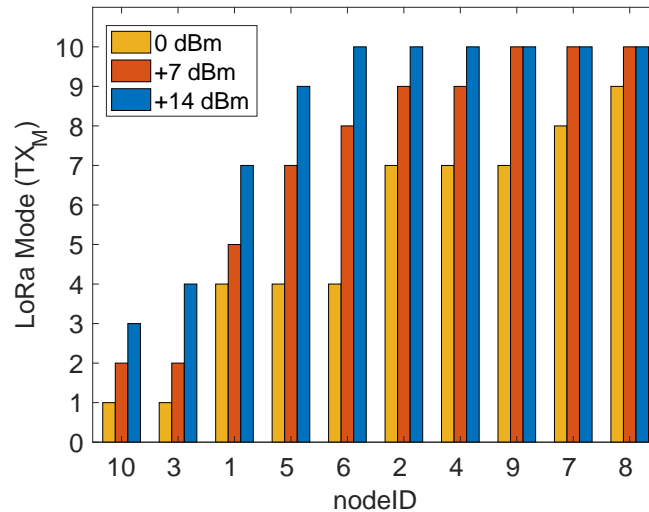
FIGURE 5.8: Minimum calculated LoRa mode per link, across different TX_P levels, for achieving at least *90* % PDR

5.3 Inter-Channel Performance Evaluation
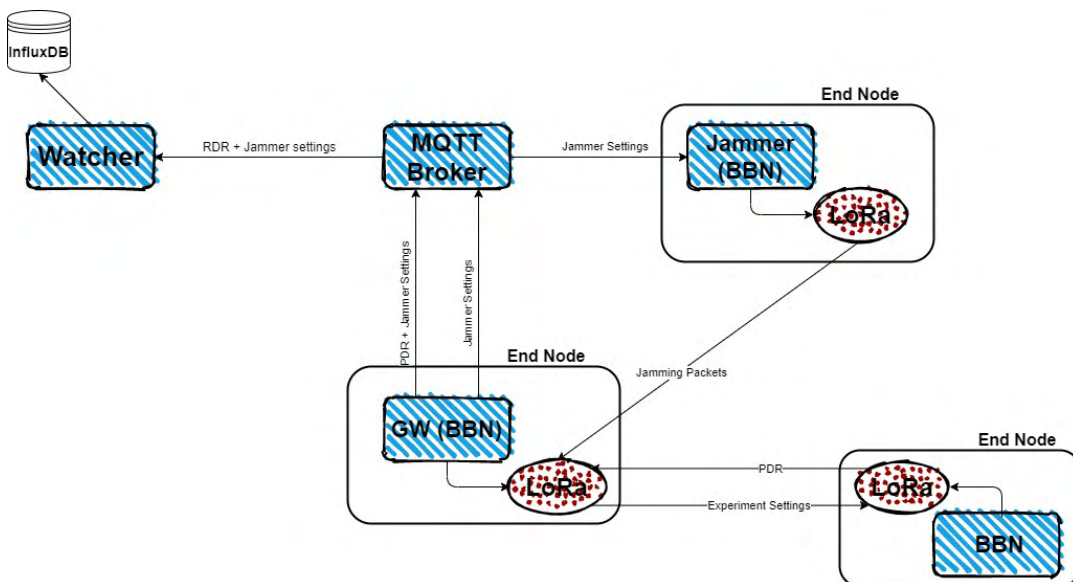
FIGURE 5.9: In-lab testbed topology

5.4 Intra-Building Performance Evaluation

In this section we present an analysis performance across a wide range of conducted in-lab testbed experiments, under uplink communication initiated from the end nodes and destined to the *GW*. In this experiments we focus to evaluate the LoRa performance under congested channels, which we emulated deploying a jammer node, and under concurrent transmissions of end nodes replicating an energy metering setup.

5.4.1 Inter-Channel Performance Evaluation

In the first experiment, we evaluate the link quality of an sx1272 transceiver when it is operating at a neighboring channel of one with high congestion. To emulate this, we use an end node at the second floor of our in-lab testbed as the uplink node, and the second end node deployed on the same floor, as a jammer node with 100% duty cycle, in neighboring channels. Specifically, the jammer node operates at *866.40 MHz*, while the evaluated uplink node operates at *866.10 MHz*. Orchestrate the uplink node and jammer node to operate on all available combinations of TX_P and TX_M corresponds to a total of 990 experimental combinations that are conducted every 14 hours, corresponding to 990 frames transmitted per execution. We execute the same experiment four times and we collect 3960 transmitted frames. In order to effectively visualize the collected measurements, we decide to plot the results in separate heat-maps based on the TX_P of the jammer node and the TX_P of uplink node.

Figures 5.10(a) and 5.10(b) illustrate the PDR performance of the uplink node on each available TX_M versus the TX_M of the jammer node. The jammer TX_M 0, in the first row of our heat-maps, indicates that in this particular round the jammer was idle and it was attach no interference to our system. We decide to spotlight this two cases as they are our extreme cases and they fully describe our best and worst case scenarios. A full presentation of our results can be found in Appendix A.
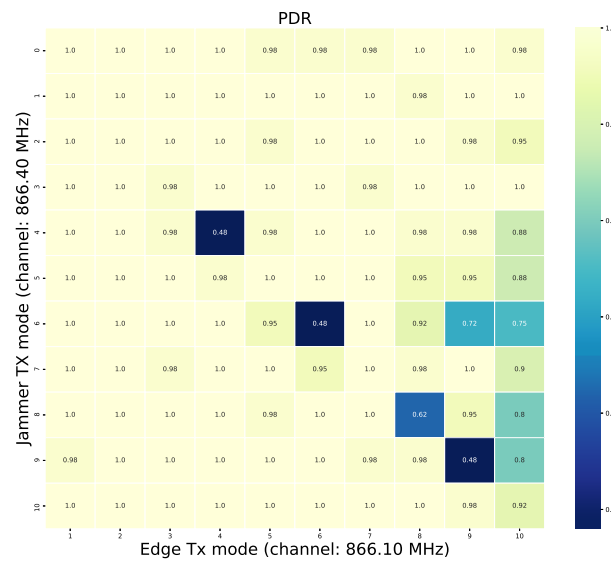
(a) PDR performance when jammer link RSSI ranges from *-79 dBm* to *-89 dBm* and the uplink RSSI ranges from *-98 dBm* to *-108 dBm*
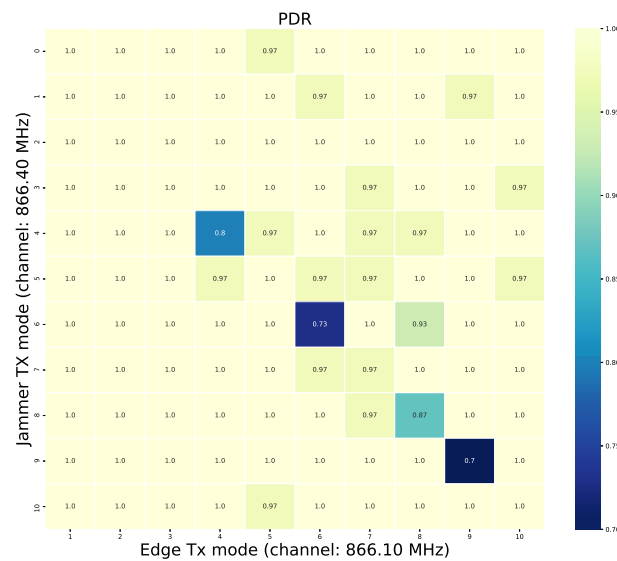
(b) PDR performance when jammer link RSSI ranges from *-98 dBm* to *-108 dBm* and the uplink RSSI ranges from *-79 dBm* to *-89 dBm*

FIGURE 5.10: LoRa PDR performance of the uplink node on each available TX_M versus the TX_M of the jammer node operating in neighboring channels

We performed the same experiments once again setting the uplink node and the jammer node to operate on the same channel (868.0 MHz). Again, figures 5.11(a) and 5.11(b) illustrate the PDR performance of the uplink node on each available

TX_M versus the TX_M of the jammer node. As before, we spotlight the same two cases as they are our extreme cases and they fully describe our best and worst case scenarios, when a full presentation of our results can be found in Appendix A.
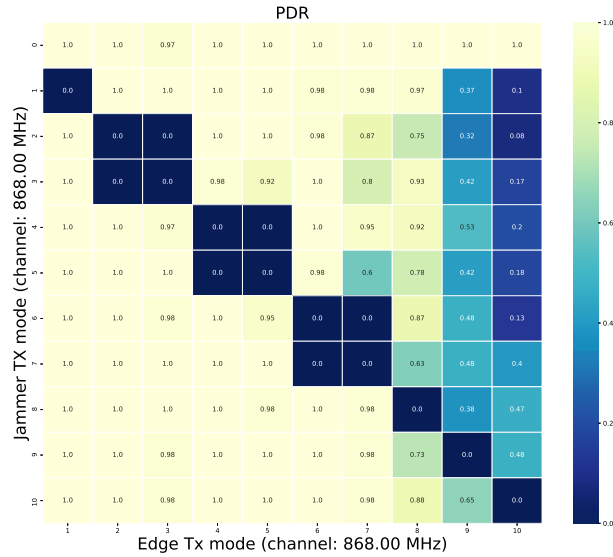
(a) PDR performance when jammer link RSSI ranges from *-79 dBm* to *-89 dBm* and the uplink RSSI ranges from *-98 dBm* to *-108 dBm*
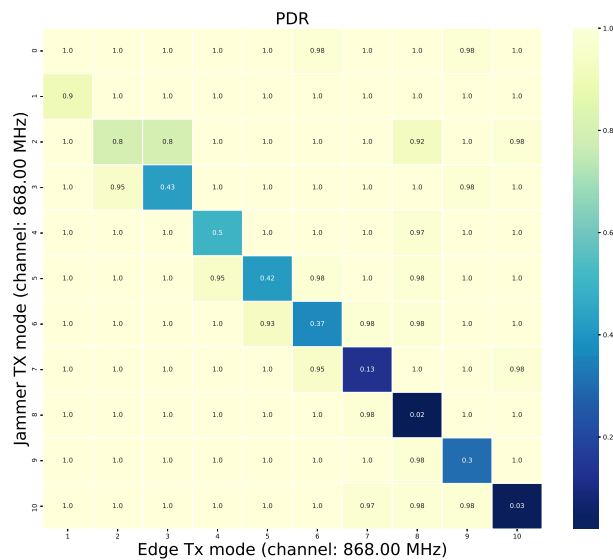
(b) PDR performance when jammer link RSSI ranges from *-98 dBm* to *-108 dBm* and the uplink RSSI ranges from *-79 dBm* to *-89 dBm*

FIGURE 5.11: LoRa PDR performance of the uplink node on each available TX_M versus the TX_M of the jammer node operating in the same channel

We can clearly observe an improvement of the PDR when the two links are not in the same channel, but still in this extreme case, where the jammer has a duty cycle of 100%, the uplink node can has low PDR as it employs faster but less reliable data rates. It is remarkable that in both cases, when the uplink's node link is stronger that the jammer link in terms of uplink RSSI, the uplink node performs better in terms of PDR. A second important finding is when the uplink node and jammer node operates in transmission modes with low bandwidth (125 or 250 KHz) there is no interference between them when they operate in different channels. As it is show in Figure 5.10(a), which is an extreme case where the uplink node has significant lower RSSI comparing to the jammer node, we can easily observe that transmission modes, as detailed in Table 3.2, with bandwidth 150 or 250 KHz have performed packet delivery ration of around 100%.

5.4.2   CSMA for LoRa Performance Evaluation

In our next experiment, we try to evaluate the link quality of an sx1272 transceiver when it is operating on a channel with high congestion. We perform two experiments where in the first one implement the CSMA/CA mechanism for collision avoidance as it is defined in IEEE 802.15.4, while in the second one we let our system to transmit packets without any mechanism for collision avoidance. To emulate a high congestion channel we deploy a jammer with 100% duty cycle. We use three nodes of our in-lab testbed as uplink nodes and particular one node from the underground floor, one from the second floor and one from the fourth floor of our building. Both the jammer node and the end nodes are operate at the same channel and specifically in 868.00 MHz. The architecture of our experiments is the same as before and illustrated in Figure 5.9 with the difference that we have three separate end nodes that are scatter in three floors of our building. The gateway instructs each time a separate end node to evaluate the link quality using our link quality evaluation framework, isolating the transmissions of each node with the others.

Orchestrating the uplink nodes and jammer node to operate on all available combinations of TX_P, TX_M and CSMA/CA (On/Off) corresponds to a total of 5580 experimental combinations that are conducted every 3 days, corresponding to 5580 frames transmitted per execution. We execute the same experiment six times and we collect 33480 transmitted frames. In order to effectively visualize the collected measurements, we decide to split the data in two groups. The first group corresponds to the data when the CSMA/CA mechanism is applied while the second one corresponds to the rest. Then we plot the results in separate heat-maps based on the TX_P of the jammer node and the TX_P of uplink node.

Figures 5.12, 5.13 and 5.14 illustrate the PDR performance of the uplink nodes from three different floors respectively on each available TX_M versus the TX_M of the jammer node. The jammer TX_M 0, in the first row of our heat-maps, indicates that in this particular round the jammer was idle and it was attach no interference to our system. The left graph represents the execution where no collision avoidance mechanism is applied while the right one represents the execution where the CSMA/CA is applied. We decide to spotlight this three cases as they are our extreme cases and they fully describe our best and worst case scenarios.
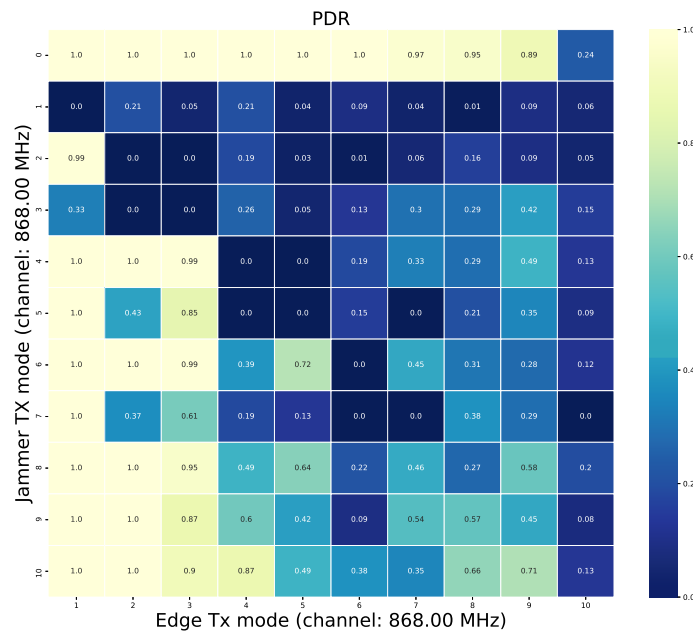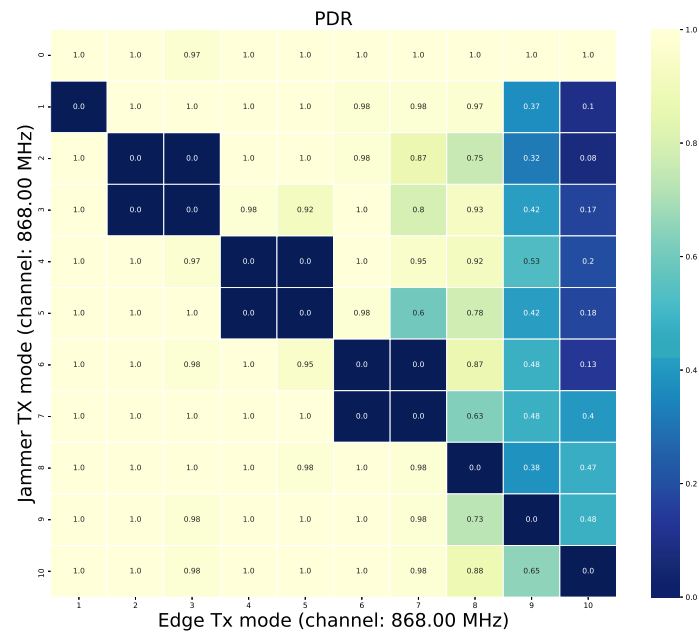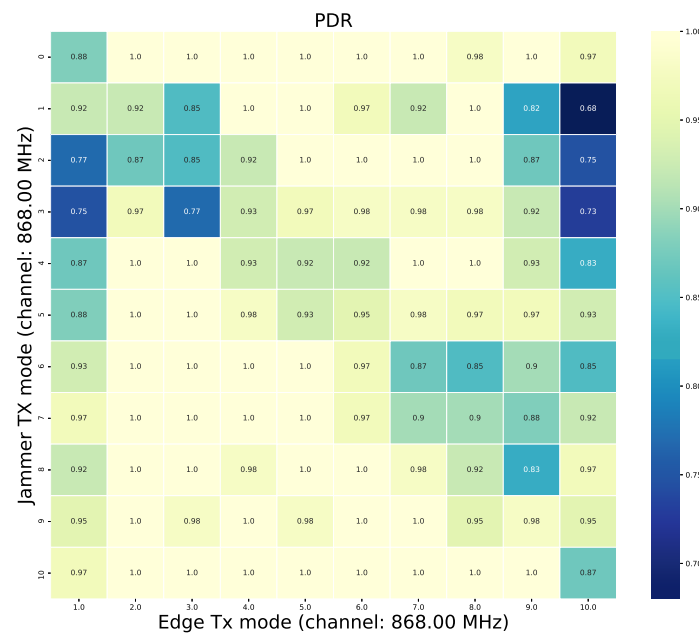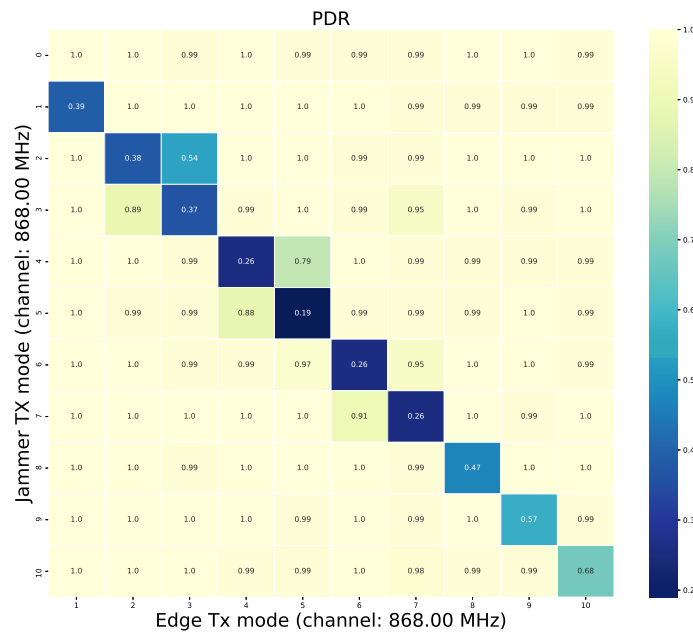
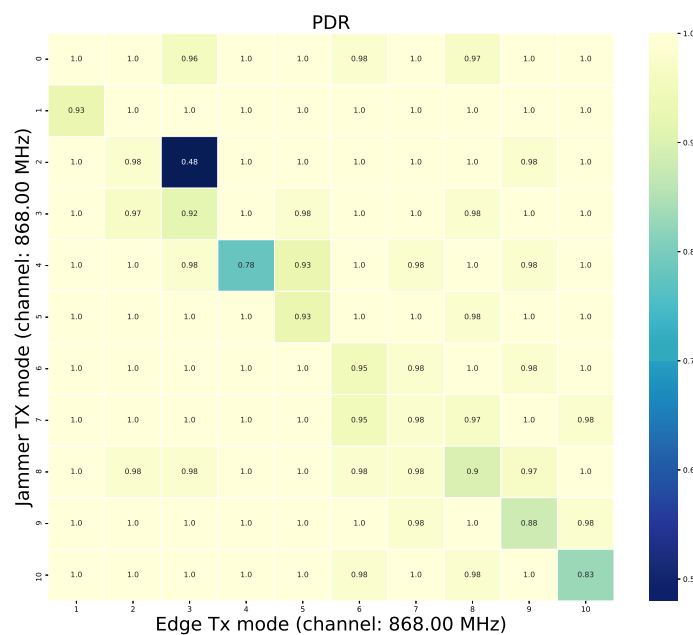(a) No CSMA/CA is applied
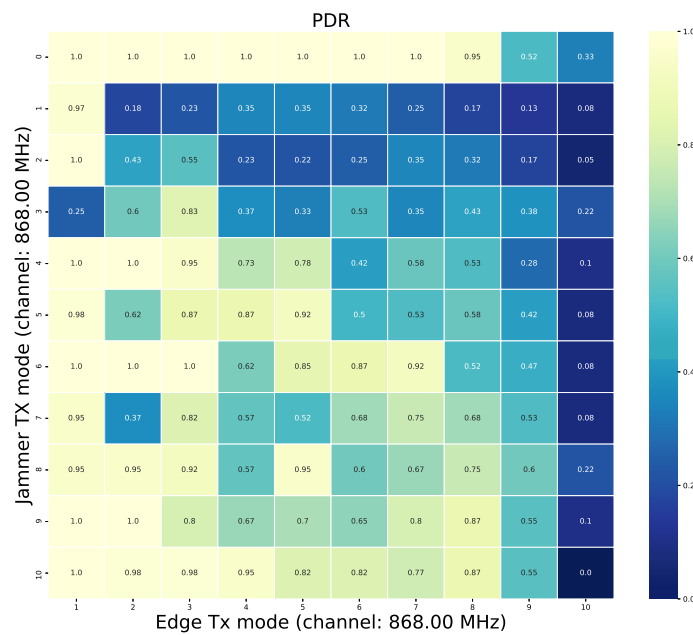
(b) CSMA/CA is applied

FIGURE 5.12: PDR comparison of CSMA/CA and no CSMA/CA approach when jammer's link RSSI ranges from *-79 dBm* to *-89 dBm* and end node's link RSSI ranges from *-120 dBm* to *-130 dBm*

(a) No CSMA/CA is applied

(b) CSMA/CA is applied

FIGURE 5.13: PDR comparison of CSMA/CA and no CSMA/CA approach when jammer's link RSSI ranges from *-79 dBm* to *-89 dBm* and end node's link RSSI ranges from *-98 dBm* to *-108 dBm*

(a) No CSMA/CA is applied

(b) CSMA/CA is applied

FIGURE 5.14: PDR comparison of CSMA/CA and no CSMA/CA approach when jammer's link RSSI ranges from *-79 dBm* to *-89 dBm* and end node's link RSSI ranges from *-87 dBm* to *-97 dBm*

We can clearly observe the improvement of packet delivery ratio even in this worst case scenarios where the jammer node has significant better link quality in terms of uplink RSSI. Figures 5.15(a) and 5.15(b) illustrate the mean PDR when the CSMA/CA mechanism is not applied and when it is applied, in the diagonal (where the jammer TX_M and uplink TX_M are the same) and on the total experiment respectively. As we can see, even with a jammer with duty cycle of 100%, the end node is able to maintain PDR higher than 90%. It is remarkable, that even in the worst case scenario where the uplink node is located on the under-ground floor of our building and the link RSSI that can achieve is lower by 31 to 51 dBM than the jammer 's link RSSI the improvement of the packet delivery ration on the uplink node is 655% on the diagonal and 44% on the total experiment respectively.

Finally, another interesting point is that even in different TX_M there is a lot of interference between the uplink node and the jammer node. Specifically, in neighboring modes 2 & 3, 4 & 5 and in modes 6 & 7, even than they have different settings regarding the bandwidth and spreading factor, they seem to behave the same.
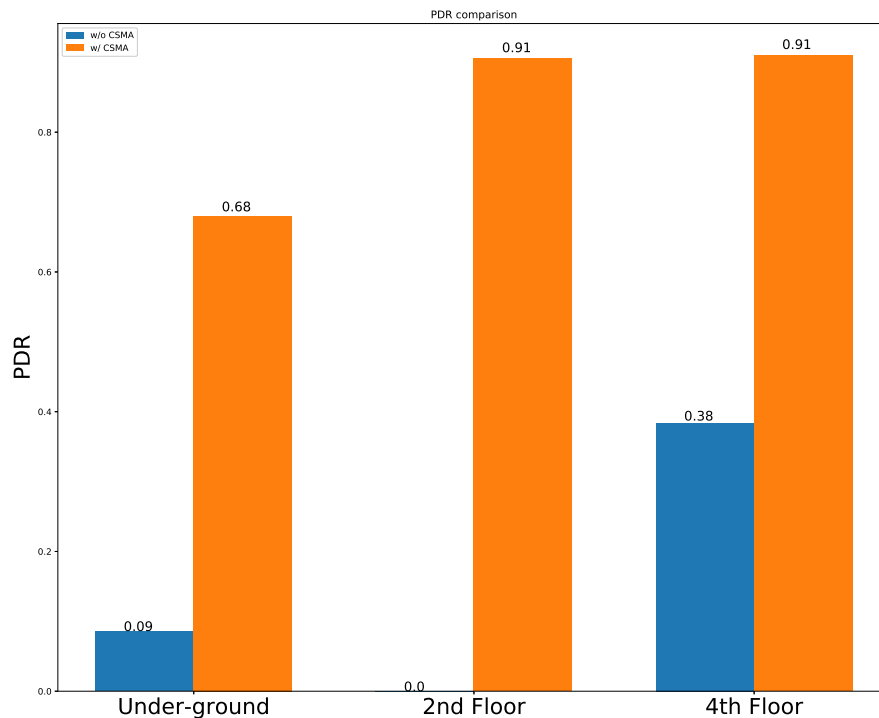
(a) Mean achieved PDR of each node when the TX_M of uplink node and jammer are the same
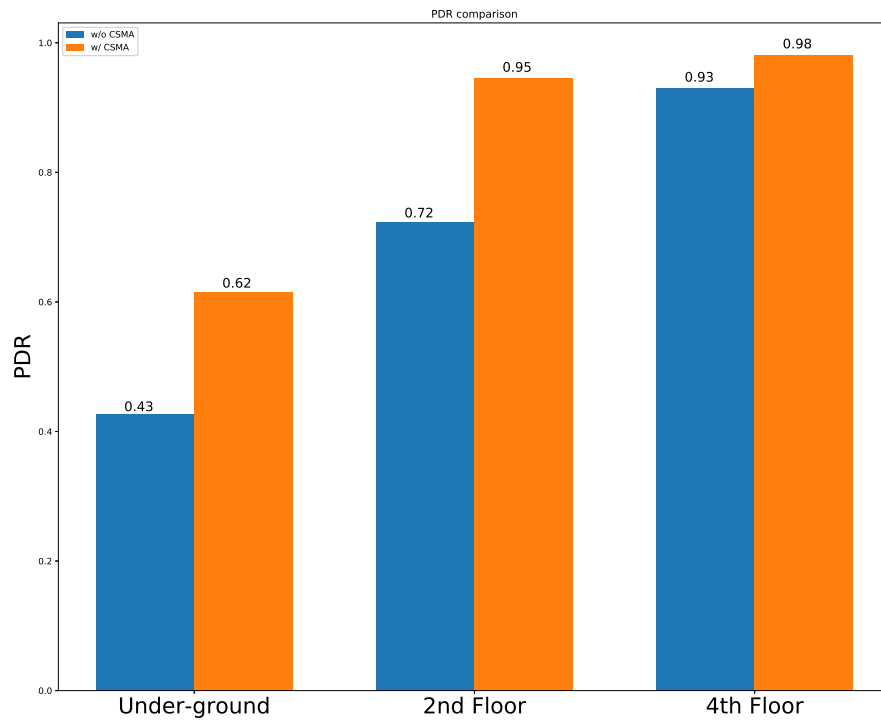
(b) Mean achieved PDR of each node on all TX_M combinations of uplink node and jammer

FIGURE 5.15: CSMA/CA performance comparison of the uplink node in terms of PDR

Chapter 6

Conclusions & Future Work

In this thesis we presented a city-wide and an in-lab monitoring LoRa-based infrastructure that provides link quality indications. Furthermore, we characterize the energy efficiency of the utilized LoRa SX1272 chipset by conducting in-depth lab experiments. We conclude that the LoRa standard is a very attractive option for deploying energy and cost efficient IoT applications in city-scale environments. Specifically, our findings indicate that rate adaptation algorithms and packet aggregation techniques can drastically benefit the energy efficiency of the LoRa protocol, when considering battery powered applications. We characterize the link performance in our city-wide testbed showing impressively high PDR at extremely low RSSI conditions, even when using high data rates.

Also, we conduct extensive experiments in our in-lab testbed in order to define the impact o concurrent transmissions in PDR when two edge nodes operate at the same or at different channels. Lastly, we evaluate the performance of LoRa protocol in terms of uplink PDR when a CSMA/CA mechanism is applied. We conclude that the LoRa protocol can achieve impressively high PDR even in a high congestion channels when the CSMA/CA mechanism is applied.

Our future directions include the expansion and the rearrangement of our testbed, so as to extend the range of collected data, specifically of low *RSSI* links and to characterize the performance of the setup across more advanced metrics, such as throughput and latency. Also the characterization of the effective energy consumption when a collision avoidance mechanism is implemented could lead to interesting findings.

Appendix A

Appendix

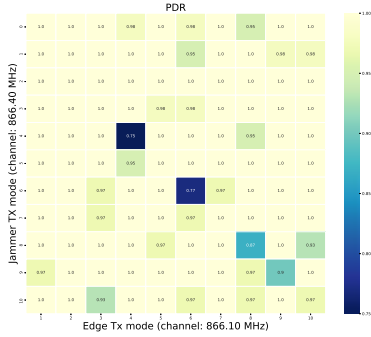(a) Edge RSSI ranges from -79 to -89dBm vs jammer RSSI that ranges from -79 to -89dBm

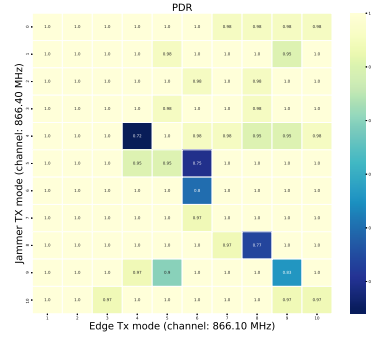(b) Edge RSSI ranges from -89 to -98dBm vs jammer RSSI that ranges from -79 to -89dBm

(c) Edge RSSI ranges from -98 to -108dBm vs jammer RSSI that ranges from -79 to -89dBm
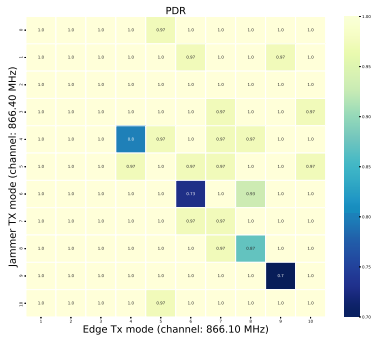
(d) Edge RSSI ranges from -79 to -89dBm vs jammer RSSI that ranges from -89 to -98dBm
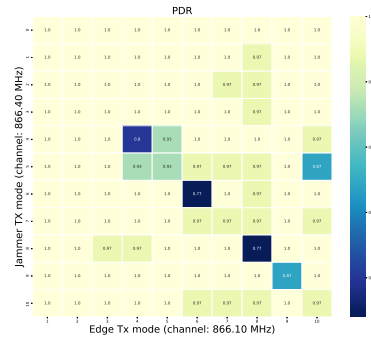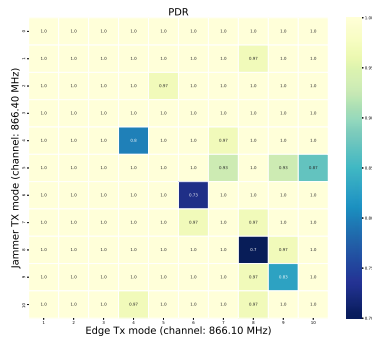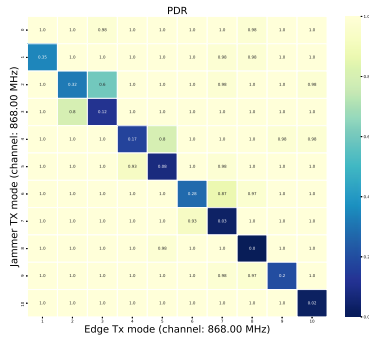
(e) Edge RSSI ranges from -89 to -98dBm vs jammer RSSI that ranges from -89 to -98dBm

(f) Edge RSSI ranges from -98 to -108dBm vs jammer RSSI that ranges from -89 to -98dBm

(g) Edge RSSI ranges from -79 to -89dBm vs jammer RSSI that ranges from -98 to -108dBm

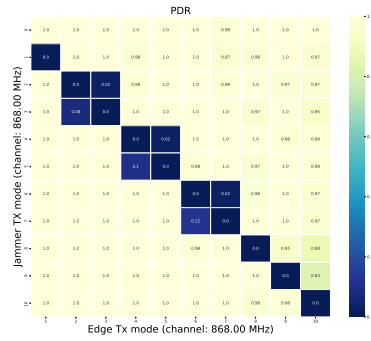(h) Edge RSSI ranges from -89 to -98dBm vs jammer RSSI that ranges from -98 to -108dBm

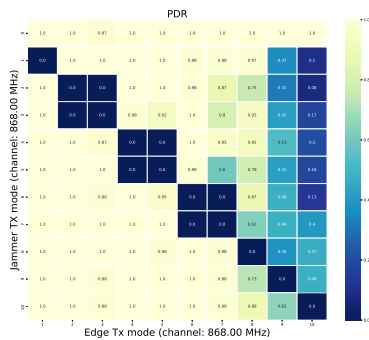(i) Edge RSSI ranges from -98 to -108dBm vs jammer RSSI that ranges from -98 to -108dBm

FIGURE A.1: LoRa TX_M evaluation in terms of PDR when an edge node operates at a neighboring channel of one with high congestion
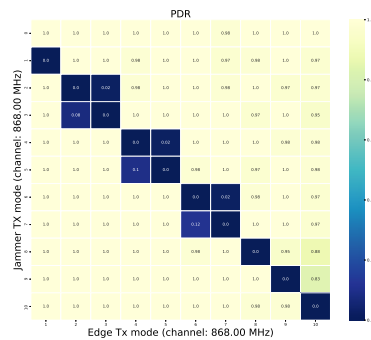
(a) Edge RSSI ranges from -79 to -89dBm vs jammer RSSI that ranges from -79 to -89dBm
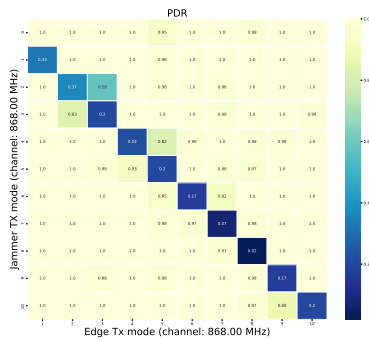

(b) Edge RSSI ranges from -89 to -98dBm vs jammer RSSI that ranges from -79 to -89dBm
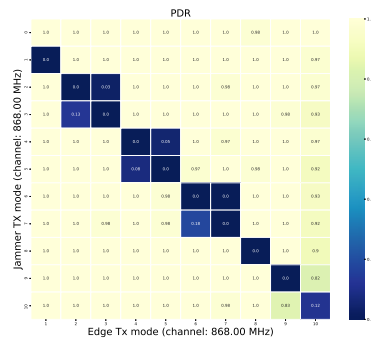

(c) Edge RSSI ranges from -98 to -108dBm vs jammer RSSI that ranges from -79 to -89dBm
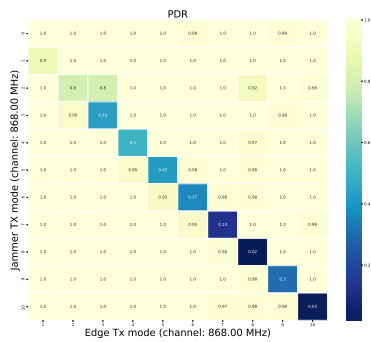

(d) Edge RSSI ranges from -79 to -89dBm vs jammer RSSI that ranges from -89 to -98dBm

(e) Edge RSSI ranges from -89 to -98dBm vs jammer RSSI that ranges from -89 to -98dBm

(f) Edge RSSI ranges from -98 to -108dBm vs jammer RSSI that ranges from -89 to -98dBm

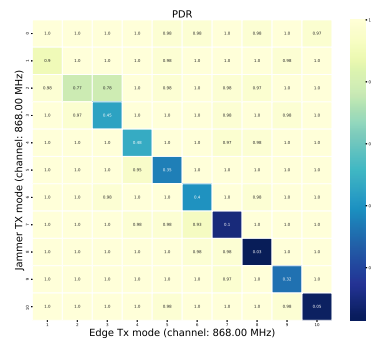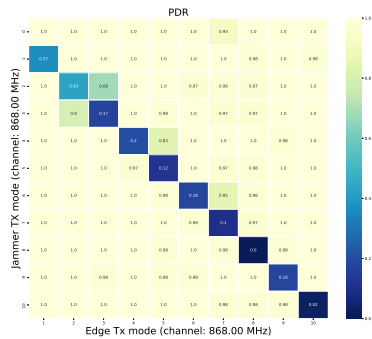(g) Edge RSSI ranges from -79 to -89dBm vs jammer RSSI that ranges from -98 to -108dBm

(h) Edge RSSI ranges from -89 to -98dBm vs jammer RSSI that ranges from -98 to -108dBm

(i) Edge RSSI ranges from -98 to -108dBm vs jammer RSSI that ranges from -98 to -108dBm

FIGURE A.2: LoRa TX_M evaluation in terms of PDR when an edge node operates on a high congestion channel

Bibliography

[1] Giannis Kazdaridis et al. "Evaluation of lora performance in a city-wide testbed: Experimentation insights and findings". In: *Proceedings of the 13th International Workshop on Wireless Network Testbeds, Experimental Evaluation & Characterization*. 2019, pp. 29–36.

[2] Giannis Kazdaridis et al. "The NITOS Wireless Sensor Network Testbed for Experimenting with Long-Range Technologies". In: *10th International Conference on the Internet of Things Companion*. 2020, pp. 1–4.

[3] Panagiotis Tzimotoudis et al. "LoRa Mesh Network Experimentation in a City-Wide Testbed". In: *Proceedings of the 13th International Workshop on Wireless Network Testbeds, Experimental Evaluation & Characterization*. 2019, pp. 49–50.

[4] Kais Mekki et al. "A comparative study of LPWAN technologies for large-scale IoT deployment". In: *ICT express* 5.1 (2019), pp. 1–7.

[5] Jean-Paul Bardyn et al. "IoT: The era of LPWAN is starting now". In: *ESSCIRC Conference 2016: 42nd European Solid-State Circuits Conference* (2016), pp. 25–30.

[6] X. Lin et al. "Positioning for the Internet of Things: A 3GPP Perspective". In: *CoRR* abs/1705.04269 (2017). eprint: 1705.04269.

[7] Sigfox. *The Global Communications Service Provider for the Internet of Things (IoT)*. https://www.sigfox.com/.

[8] DASH7 Alliance. *DASH7 Alliance - An open specification*. https://dash7-alliance.org/.

[9] Weightless. *Weightless - Setting the standard for IoT*. http://www.weightless.org/.

[10] A. Hoglund et al. "Overview of 3GPP Release 14 Enhanced NB-IoT". In: *IEEE Network* 31.6 (2017), pp. 16–22.

[11] A. Hoglund et al. "Overview of 3GPP Release 14 Further Enhanced MTC". In: *IEEE Communications Standards Magazine* 2.2 (2018), pp. 84–89.

[12] F. Adelantado et al. "Understanding the Limits of LoRaWAN". In: *IEEE Communications Magazine* 55.9 (2017), pp. 34–40.

[13] Laurens Slats. *Inside Out Semtech's Corporate Blog*. http://tiny.cc/4qutsz. Jan. 2020.

[14] Semtech. *SX1272/73, 860 MHz to 1020 MHz Low Power Long Range Transceiver*. http://tiny.cc/2qutsz. Rev. 4, Jan. 2019.

[15] Semtech. *SX1276, 137 MHz to 1020 MHz Long Power Low Range Transceiver*. http://tiny.cc/zputsz. Rev. 7, May. 2020.

[16] Semtech. *SX1301, Digital Baseband Chip for outdoor LoRaWAN® macro gateways*. http://tiny.cc/wqutsz. Rev. 2.4, June 2017.

[17] *LoRa Alliance*. http://tiny.cc/fqutsz.

[18] LoRa Alliance. "LoRaWAN 1.1 regional parameters". In: *technical specification* (2017).

[19] ERM PR08 ETSI. "EN 300 220-1: Electromagnetic compatibility and Radio spectrum Matters (ERM); Short Range Devices (SRD); Radio equipment to be used in the 25 MHz to 1000 MHz frequency range with power levels ranging up to 500 mW". In: *ETSI, France* (2012).

[20] LoRa Alliance. *LoRaWAN® Specification v1.0.3*. July, 2018.

[21] LoRa Alliance. *LoRaWAN® Backend Interfaces Specification v1.0*. Oct., 2017.

[22] Luis Sanchez et al. "SmartSantander: IoT experimentation over a smart city testbed". In: *Computer Networks* 61 (2014). Special issue on Future Internet Testbeds - Part I.

[23] Stefan Bouckaert et al. "The w-iLab.t testbed". In: *Proc. of TridentCom '10*. 2010.

[24] C. Adjih et al. "FIT IoT-LAB: A large scale open experimental IoT testbed". In: *Proc. of WF-IoT '15*. 2015.

[25] Roman Lim et al. "FlockLab: A Testbed for Distributed, Synchronized Tracing and Profiling of Wireless Embedded Systems". In: *Proc. of IPSN '13*. 2013.

[26] BeagleBone Black. *https: // goo. gl/ jkfCcL*. *[Accessed 27-June-2019]*.

[27] LoRa SX1272 Networking Guide Libelium's. *http: // tinyurl. com/ y6nrb877*. *[Accessed 27-June-2019]*.

[28] G. Kazdaridis et al. "Nano-Things: Pushing Sleep Current Consumption to the Limits in IoT Platforms". In: *Proc. of IoT '20*. 2020.

[29] *RF Solutions*. https://www.rfsolutions.co.uk/.

[30] G. Kazdaridis et al. "EVERUN: Enabling Power Consumption Monitoring in Underwater Networking Platforms". In: *Proc. of the 11th Workshop on WiN-TECH*. ACM. 2017, pp. 83–90.

[31] Stratos Keranidis et al. "Online Energy Consumption Monitoring of Wireless Testbed Infrastructure Through the NITOS EMF Framework". In: *Proc. of WiN-TECH '13*.

[32] G. Kazdaridis et al. "Demo: In-situ Power Consumption Meter for Sensor Networks Supporting Extreme Dynamic Range". In: *Proc. of WiNTECH '17*. 2017.

[33] Thanh-Hai To and Andrzej Duda. "Simulation of lora in ns-3: Improving lora performance with csma". In: *2018 IEEE International Conference on Communications (ICC)*. IEEE. 2018, pp. 1–7.

[34] Muhammad Omer Farooq and Dirk Pesch. "A search into a suitable channel access control protocol for lora-based networks". In: *2018 IEEE 43rd Conference on Local Computer Networks (LCN)*. IEEE. 2018, pp. 283–286.

[35] Shahzeb Ahsan et al. "Improving Channel Utilization of LoRaWAN by using Novel Channel Access Mechanism". In: *2019 15th International Wireless Communications & Mobile Computing Conference (IWCMC)*. IEEE. 2019, pp. 1656–1661.

[36] Congduc Pham. "Investigating and experimenting CSMA channel access mechanisms for LoRa IoT networks". In: *2018 IEEE Wireless Communications and Networking Conference (WCNC)*. IEEE. 2018, pp. 1–6.

[37] G. Kazdaridis et al. "In-situ Power Consumption Meter for Sensor Networks supporting Extreme Dynamic Range". In: *Proc. of the 11th Workshop on WiN-TECH*. 2017.

[38]   R. Khereddine et al. "Adaptive logical control of RF LNA performances for efficient energy consumption". In: *IFIP/IEEE Int. Conf. on Very Large Scale Integration-System on a Chip*. Springer. 2010.

[39]   S. Keranidis et al. "Experimental Evaluation and Comparative Study on Energy Efficiency of the Evolving IEEE 802.11 Standards". In: *Proceedings of the 5th Int. Conf. on Future Energy Systems*. e-Energy '14. 2014.

[40]   S. Keranidis et al. "Online energy consumption monitoring of wireless testbed infrastructure through the NITOS EMF framework". In: *Proc. of the 8th ACM int. workshop on WiNTECH*. ACM. 2013.

[41]   SX1272/73 860 MHz to 1020 MHz Low Power Long Range Transceiver. Rev. 3.1 March 2017. *http: // tiny. cc/ tw8w8y*. *[Accessed 27-June-2019]*.